15. Nakata K, Shino K, Hamada M, Mae T, Miyama T, Shinjo H, Horibe S, Tada K, Ochi T, Yoshikawa H. Human meniscus cell: characterization of the primary culture and use for tissue engineering. *Clin Orthop Relat Res* 2001;**391**(Suppl.): S208–18.
16. Nitzan DW. Intraarticular pressure in the functioning human temporomandibular joint and its alteration by uniform elevation of the occlusal plane. *J Oral Maxillofac Surg* 1994;**52**:671–80.
17. Nitzan DW. The process of lubrication impairment and its involvement in temporomandibular joint disc displacement: a theoretical concept. *J Oral Maxillofac Surg* 2001;**59**:36–45.
18. Ritchlin C, Fibroblast biology. Effector signals released by the synovial fibroblast in arthritis. *Arthritis Res* 2000;**2**:356–60.
19. Takahashi K, Kubo T, Goomer RS, Amiel D, Kobayashi K, Imanishi J, Teshima R, Hirasawa Y. Analysis of heat shock proteins and cytokines expressed during early stages of osteoarthritis in a mouse model. *Osteoarthritis Cartilage* 1997;**5**:321–9.
20. Tanaka E, Rodrigo DP, Miyawaki Y, Lee K, Yamaguchi K, Tanne K. Stress distribution in the temporomandibular joint affected by anterior disc displacement: a three-dimensional analytic approach with the finite-element method. *J Oral Rehabil* 2000;**27**:754–9.
21. Tanaka E, Del Pozo R, Sugiyama M, Tanne K. Biomechanical response of retrodiscal tissue in the temporomandibular joint under compression. *J Oral Maxillofac Surg* 2002; **60**:546–51.

Address:
Yutetsu Akamine
Second Department of Oral and Maxillofacial Surgery
Osaka Dental University Graduate School of Dentistry 8-1
Kuzuha Hanazonocho
Hirakata
Osaka
573-1121
Japan
Tel: +81 72 864 3111; Fax: +81 72 864 3000
E-mail: akamine-you@aroma.ocn.ne.jp

Osteoarthritis and Cartilage 20 (2012) 296–304

Osteoarthritis and Cartilage

Three-dimensional distribution of articular cartilage thickness in the elderly talus and calcaneus analyzing the subchondral bone plate density

K. Akiyama †, T. Sakai ‡*, N. Sugimoto §, H. Yoshikawa ‡, K. Sugamoto †

† *Department of Orthopaedic Biomaterial Science, Osaka University Graduate School of Medicine, Suita, Japan*
‡ *Department of Orthopaedic Surgery, Osaka University Graduate School of Medicine, Suita, Japan*
§ *Sugimoto Data Analysis Service, Nagoya, Japan*

ARTICLE INFO

Article history:
Received 2 December 2011
Accepted 27 December 2011

Keywords:
Cartilage thickness
Subchondral bone density
Talus
Calcaneus
3D-digitizer
Computed tomography

SUMMARY

Objective: To unveil the three-dimensional (3D) distribution of talocrural and posterior subtalar articular cartilage thickness in the elderly cadavers using 3D computed tomography (CT) and a 3D-digitizer and to evaluate the relationship between subchondral bone plate density and the overlying cartilage thickness.
Design: Sixteen tali and 16 calcanei from eight cadavers were scanned with 3D-CT to create bone surface models, and with a 3D-digitizer to make cartilage surface models. These two surface models were merged using surface registration method. Articular cartilage thickness was evaluated as the distance between the two models, and the distribution was mapped. The anatomic cartilage thickness of five tali and five calcanei was compared with the distance between the cartilage and bone surface models to calculate optimum threshold for extracting the subchondral bone plate. Generalized estimating equations were used for comparison and measurement errors. Canonical correlation analysis was performed to determine the strength of association between subchondral bone plate threshold and cartilage thickness.
Results: The talar-subtalar articular cartilage tended to be the thickest of the three joints. In the talocrural joint, the anterior region was the thinnest, and increasing cartilage thickness was seen toward the posterior. In the talar-subtalar joint, the central region was the thickest. Mean measurement errors were 0.059 ± 0.066 mm, 0.038 ± 0.040 mm, and 0.018 ± 0.065 mm in the talocrural, talar-subtalar, and calcaneal-subtalar joints, respectively. The canonical correlation coefficient was 0.995 ($P < 0.001$).
Conclusions: The articular cartilage thickness was distributed in the elderly hindfoot. The subchondral bone plate density was significantly correlated with the anatomic cartilage thickness.

Introduction

The etiology of primary ankle and subtalar osteoarthritis (OA) has not been fully elucidated. In human locomotion, the ankle and subtalar joint have an important role in the complex biomechanics of the hindfoot[1]; however, there is little information regarding the distribution of cartilage thickness in ankle joints of elderly individuals[2] or no clear reference of subtalar cartilage distribution. Accurate knowledge of three-dimensional (3D) distribution of ankle and subtalar cartilage thickness is important to evaluate both ankle and subtalar OA development and biomechanics.

The subchondral bone plate provides a linkage between hyaline cartilage and cancellous bone[3]. It has been regarded as a morphological and mechanical unit and plays an important role in attenuating the impact forces typically encountered during dynamic joint loading[4–6]. Changes in subchondral bone structure and density have been considered to reflect loading history in diarthrodial joints and progression of OA[7–9]. Besides, OA related subchondral bone changes are thought to initiate and accelerate cartilage degeneration by increasing the mechanical stiffness of subchondral bone and leading to more energy being transferred through the overlying cartilage[10]. Although several studies have reported on subchondral trabecular bone[11,12] and on the density of subchondral bone marrow below the subchondral bone plate[13,14], there is little information on the density of subchondral bone plate itself. Investigating the relationship between the density of the subchondral bone plate and the overlying cartilage thickness may be necessary for understanding the development of OA[15].

* Address correspondence and reprint requests to: T. Sakai, Department of Orthopaedic Surgery, Osaka University Graduate School of Medicine, 2-2, Yamadaoka, Suita 565-0871, Japan. Tel: 81-6-6879-3552; Fax: 81-6-6879-3559.
E-mail addresses: k.aki@hotmail.co.jp (K. Akiyama), tsakai-osk@umin.ac.jp (T. Sakai), webmaster@snap-tck.com (N. Sugimoto), yhideki@ort.med.osaka-u.ac.jp (H. Yoshikawa), sugamoto@ort.med.osaka-u.ac.jp (K. Sugamoto).

1063-4584/$ – see front matter
doi:10.1016/j.joca.2011.12.014

It is important to take the threshold value into consideration when using computed tomography (CT) arthrography to evaluate articular cartilage thickness because extraction of the subchondral bone from CT images is dependent on the threshold[16]. The density of subchondral bone plate in the femoral head of elderly specimens was reported to be 480 Hounsfield units (HU) with a unique technique using 3D-CT and a contact-type 3D-digitizer[16], a 3D data acquisition device that can capture a multitude of orthogonal coordinates on the surface of physical objects by contacting the surface[16–20].

The purpose of the present study was to unveil the 3D distribution of talocrural and posterior subtalar articular cartilage thickness in the elderly cadavers using 3D-CT and a 3D-digitizer, to confirm the optimum threshold for the talus and calcaneus, and to evaluate the relationship between subchondral bone plate density and cartilage thickness.

Methods

Specimens and study design

Sixteen tali and 16 calcanei from eight cadavers embalmed in formalin were harvested. The cadavers included seven women and one man, with a mean age of 89 years (range, 74–96 years). Anthropometric data were not obtained. Exclusion criteria were as follows: fracture, previous surgery, and degenerative disease which was defined as presence of osteophyte, damage to the articular cartilage surface, and exposure of the subchondral bone. Consequently, all recruited bones were enrolled. It was confirmed that the cadavers had no symptoms of ankle joint or foot disorders, or any history of such disorders according to the clinical records. As landmarks for integration of each digitized data set and for surface registration, five high-carbon chromium-bearing steel spheres with a high-tolerance radius (4.00 ± 0.005 mm) were glued firmly with cyanoacrylate cement to the bone surface of each talus and calcaneus, excluding the talocrural and subtalar articular areas because Neu *et al.*[21] reported that when four or more markers were used, the standard deviation of the rotation and translation parameters was less than 0.1% of the mean. A previous study validated the accuracy and reproducibility of the present method[16].

The 3D coordinates of surface points of the articular cartilage and of all the steel spheres were measured using a contact-type 3D-digitizer (Cyclone, Renishaw, New Mills, UK) with a spherical sensor fixed on the probe tip, with accuracy of <50 μm[16–18]. All specimens were fixed to the measuring table with strong industrial adhesive so that the articular surface faced upwards and was firmly secured during scanning (Fig. 1). The digitizing device enables measurement of parallel slices at intervals of 0.5 mm on the articular cartilage surface and the steel balls. During scanning, sets of 3D scattered points, called "point clouds," were obtained from two or three viewpoints.

A two detector-row CT scanner (SOMATOM Spirit, Siemens, Erlangen, Germany) was used for helical axial image acquisition of each specimen with steel spheres. The following standardized protocol was used: 130 kV, 54 mA, collimation of 1.0 mm, a pitch of 1, and a rotation length of 1.0 s. Reconstructions were obtained using 1.0-mm sections, a 0.5-mm increment, a Kernel B60 filter, a 100-mm field of view, and a 512×512 matrix.

Integrated repeatability of data acquisition of the 3D-digitizer and 3D-CT was previously reported[16] to have an intraclass correlation coefficient (ICC) of 0.94.

Image processing

Point-clouds of data obtained from the 3D-digitizer were saved in ASCII format, and Imageware software (UGS Inc., Plano, TX, USA) was used for preprocessing. Using the Imageware selection tools, the different point-clouds of data from two or three viewpoints were merged into one set of point data for each subject to create surface models of the tali and calcanei, including cartilage surface models. The surface model data from the 3D-digitizer were transferred to processing software (Magics, Materialise, Leuven, Belgium) in STL file format[22]. Magics was also used to extract surface models of the steel balls for each talus and calcaneus.

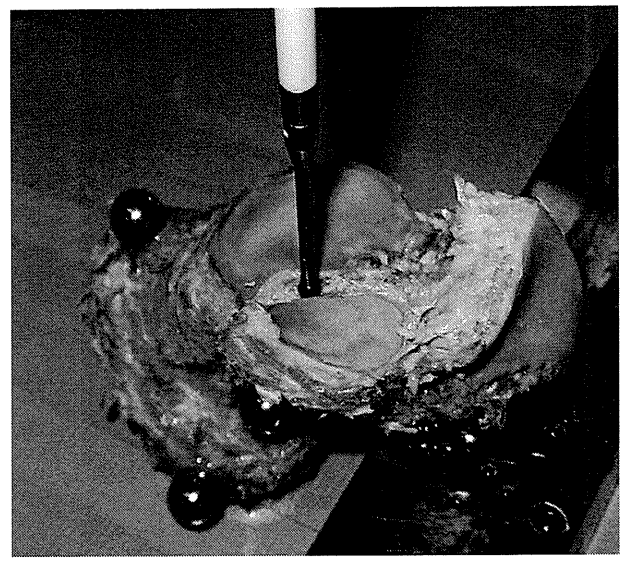

Fig. 1. All specimens were fixed and digitized such that the articular surfaces of interest faced upwards.

The CT data were saved in a standard digital imaging and communications in medicine (DICOM) format and imported into the Virtual Place M software (Medical Imaging Laboratory, Tokyo, Japan). Two different surface models were created from the same CT data using fully automated segmentation. First, thresholds of 439 HU, 532 HU, and 480 HU defined in 'Determination of optimum threshold' were set to exclude calcification and mineralization in soft tissue and to extract talar-talocrural, talar-subtalar, and calcaneal-subtalar subchondral bone, respectively. Second, for surface registration, a threshold of 7,500 HU was set to extract the steel balls but not bone surface. All surface models were saved in VTK format and visualized using original software with all programs written in Visual C++ (Orthopedics Viewer; Osaka University, Suita, Japan)[23].

Surface registration

The iterative closest point (ICP) algorithm[24], a well-developed method for surface registration, was used to register the 3D surface model and the set of 3D points. From the initial transformation parameters, optimal parameters were found while minimizing the sum of the distance from each 3D point to the surface. For each specimen, the surface models of steel balls from CT data were registered with those from the digitized data. The bone surface model from the CT data and the cartilage surface model from the digitized data were then merged with reference to the steel ball registration to produce the inferred 3D cartilage thickness (Fig. 2). The reproducibility of the surface registration based on spheres in space had been previously reported to be high[16], where the ICC was 0.99.

Proximity mapping

Articular cartilage thickness between bone and cartilage surface models was measured using an established proximity mapping

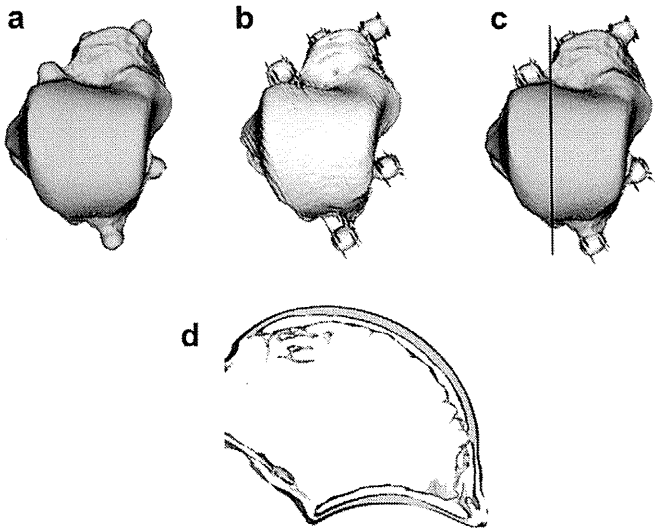

Fig. 2. Surface models of a left talus. (a) Surface model obtained using the 3D-digitizer, showing the talocrural cartilage surface. (b) Surface model obtained from 3D-CT in the same specimen, showing the talocrural subchondral bone surface. (c) Registration of the two models by surface registration of the steel spheres. The black line indicates sectioning of the talus. (d) Cross-section along the line shown in (c). The inferred cartilage is colored pink.

method[16,25]. Proximity mapping demonstrates the distances between these two 3D surface models. A custom program was created to measure intermodal distances using the output file from the solid model formation (3D reconstruction), which gives all vertices positions of individual surface triangles that form the surface of the reconstructed bone or cartilage in space.

The vertices of the triangles were used as discrete bony or cartilaginous landmarks and as starting points for estimating the minimum distance between subchondral bone and cartilage. The algorithm calculated the minimum distance from a specific vertex of a surface model to the surface cell of the counterpart. An output file was created that contains the minimum distance between each vertex and the adjacent model to which it corresponds. This program was written to calculate the area of one bone or one cartilage surface with respect to another within a user-specified threshold distance; the proximity maps in the present study were calculated at intervals of 0.5 mm (Figs. 3–5).

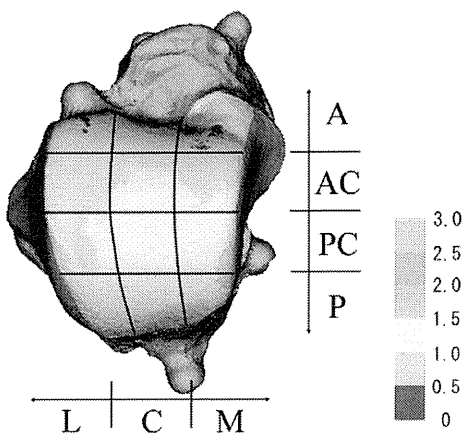

Fig. 3. 3D distribution of talocrural articular cartilage thickness of the talus shown in Fig. 2 using the proximity mapping method. The color scale is in millimeters (A, anterior; AC, anterocentral; PC, posterocentral; P, posterior; M, medial; C, central; and L, lateral).

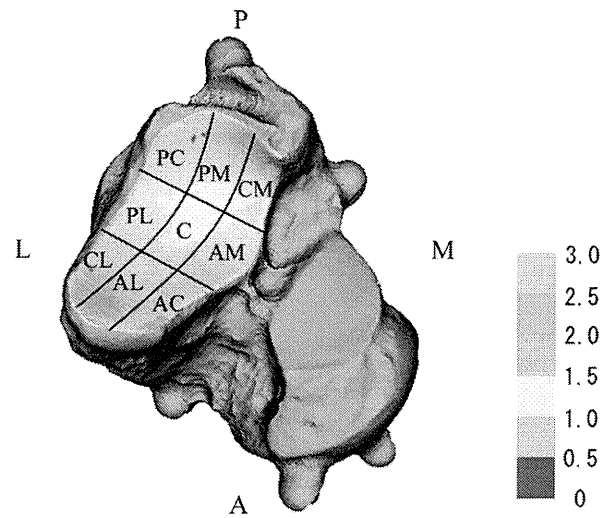

Fig. 4. 3D distribution of posterior subtalar articular cartilage thickness of the talus shown in Fig. 2, using the proximity mapping method. The color scale is in millimeters (A, anterior; P, posterior; M, medial; L, lateral; AM, anteromedial; AC, anterocentral; AL, anterolateral; CM, centromedial; C, central; CL, centrolateral; PM, posteromedial; PC, posterocentral; and PL, posterolateral).

Data analysis

Each talocrural cartilage surface was divided into 12 regions. In the anterior-posterior direction, the cartilage layers were evenly divided into four parts. In the medial-lateral direction, the cartilage layers were evenly divided into three parts (Fig. 3). Because the rectangular cartilage surface of posterior subtalar joint is located obliquely for anterior-posterior or medial-lateral direction, each rectangular cartilage surface was divided into nine regions as depicted in Figs. 4 and 5. In each divided region, mean and maximum cartilage thickness, and standard deviation were calculated. All data were analyzed by an author (KA).

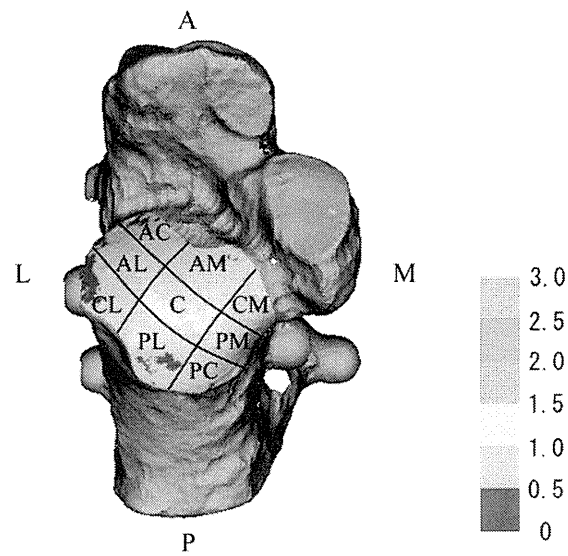

Fig. 5. 3D distribution of posterior subtalar articular cartilage thickness of a left calcaneus, using the proximity mapping method. The color scale is in millimeters (A, anterior; P, posterior; M, medial; L, lateral; AM, anteromedial; AC, anterocentral; AL, anterolateral; CM, centromedial; C, central; CL, centrolateral; PM, posteromedial; PC, posterocentral; and PL, posterolateral).

Determination of optimum threshold

Five tali and five calcanei were unilaterally obtained from one male and four female cadavers embalmed in formalin (mean age, 84 years; range, 76–93 years). Macroscopically, there were no abnormalities in the articular cartilage of all specimens. Each subject was sectioned into halves: one cross-section was for anatomic evaluation, and the other was for the 3D-digitizer and 3D-CT analysis (Fig. 6).

For each half-specimen, the anatomic articular cartilage thickness was manually measured from cartilage surface to the chondro-osseous junction using a stereomicroscope (AZ-100, Nikon, Tokyo, Japan) and a digital template. Concerning the reproducibility of calculating with the stereomicroscope, a previous study[16] reported that the ICC was 0.99 and the mean error of measurement was 0.011 ± 0.020 mm.

The other half-specimen with five steel spheres was digitized by the 3D-digitizer and scanned with 3D-CT with the cross-section perpendicular to the scanning plane. Eighteen thresholds (50–900 HU) were set at intervals of 50 HU in the software and 18 bone surface models were made in each specimen. The cartilage surface model by the 3D-digitizer and each bone ones were merged with the surface registration to create 18 kinds of inferred cartilage thickness for each articular specimen. Thirty observation points were evenly placed on the cross-section of the cartilage surface model for comparing the inferred cartilage thickness of surface models with the anatomic counterpart. The inferred cartilage thickness of surface models was measured by the 0.01 mm as the minimum distance from the observation point to the surface of bone models (Fig. 6).

First, at each observation point, the local threshold of subchondral bone plate was determined at intervals of 50 HU by comparing the 18 kinds of inferred cartilage thickness with the anatomic section. Next, 30 local threshold values in each articular specimen were averaged to calculate the proper threshold. Then, each five proper threshold values in talocrural, talar-subtalar, or calcaneal-subtalar surface were averaged to determine the optimum threshold in the articular surface.

Statistics

The mean articular cartilage thickness was compared between the talocrural, the talar-subtalar, and the calcaneal-subtalar joint with generalized estimating equations (GEE) with articular surfaces and bilateral measurements as the within-subject factors, followed by a *post hoc* Bonferroni multiple comparison test.

The mean and maximum articular cartilage thickness was compared among 12 regions in the talocrural joint and nine regions in the talar- and calcaneal-subtalar joints. Each comparison was performed with GEE with regions and bilateral measurements as the within-subject factors, followed by a *post hoc* Bonferroni multiple comparison test.

When using the optimum threshold for five tali and five calcanei in 'Determination of optimum threshold', the mean measurement errors including 95% confidence intervals (CI) between anatomic cartilage thickness and the inferred cartilage thickness of surface models were calculated in each articular surface using GEE with observation points and the way of calculating cartilage thickness (anatomic slices or surface models) as the within-subject factors.

Canonical correlation analysis (CCA) was used to determine the strength of association between the subchondral bone plate density and the overlying anatomic cartilage thickness. CCA is a multivariate correlation technique that investigates the interrelationships between multiple independent and multiple dependent variables[26,27]. Using the proper threshold values as independent variables and the mean anatomic cartilage thickness as dependent variables in the talocrural and talar-subtalar joint, canonical correlation coefficient was calculated.

Statistical analyses were conducted using SPSS for Windows (version 19.0; IBM, Armonk, NY, USA) and statistical significance was accepted for P values of <0.05.

Results

The cartilage thickness distributions from one typical subject's talocrural, posterior talar-subtalar, and posterior calcaneal-subtalar joint surfaces are shown in Figs. 3–5, respectively. Mean cartilage thickness was 0.82 ± 0.12 mm, 0.98 ± 0.16 mm, and 0.75 ± 0.12 mm in talocrural, talar-subtalar, and calcaneal-subtalar joint, respectively. Mean cartilage thickness of the talar-subtalar joint was significantly thicker than that of the talocrural of the talus ($P = 0.045$) and that of the calcaneal-subtalar ($P < 0.001$).

Comparison of cartilage thickness among the regions in each articular surface showed significant differences. In the talocrural surface, the mean and maximum cartilage thickness tended to be the largest in the posterolateral and in the posterocentral-medial

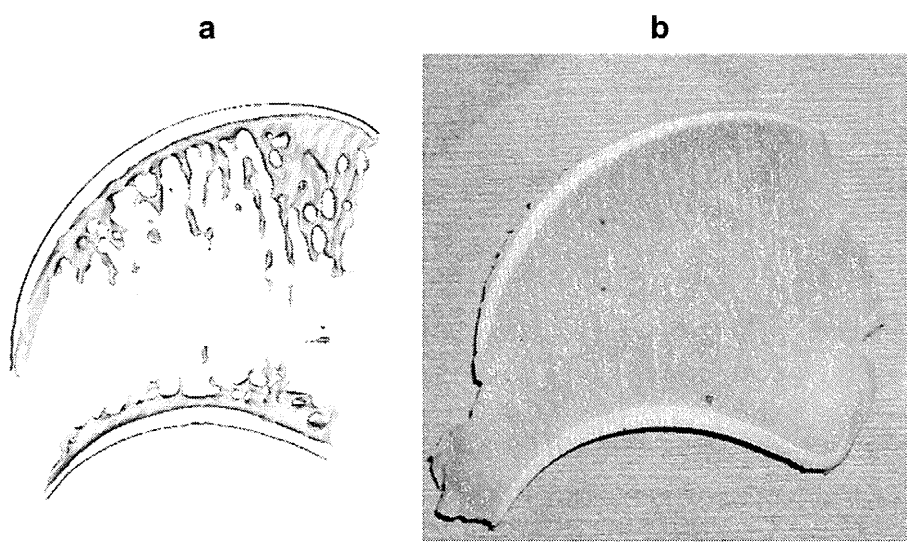

Fig. 6. (a) Cross-section of the surface model of a talus made by 3D-digitizer and 3D-CT, showing inferred cartilage thickness. (b) Anatomic counterpart section.

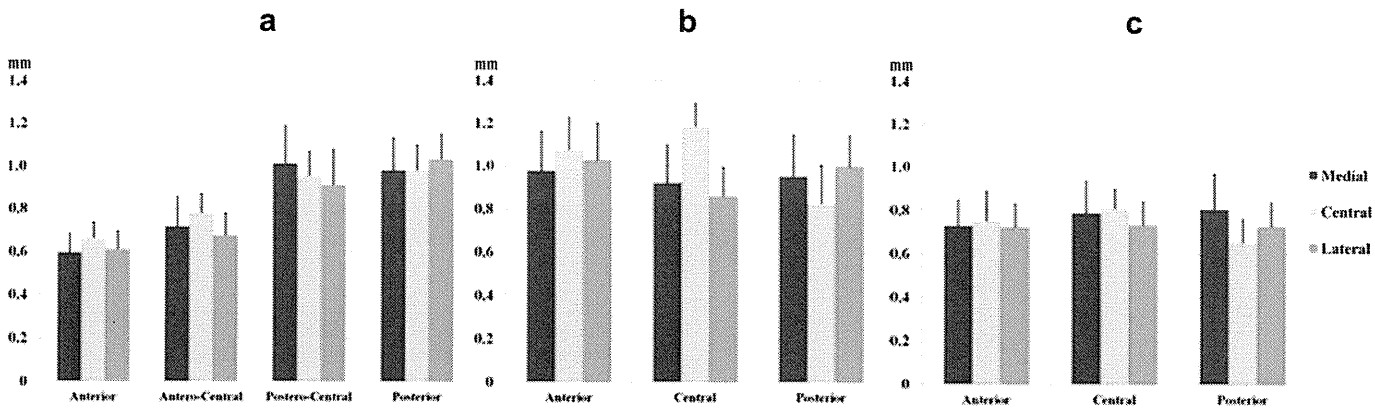

Fig. 7. Bar charts showing mean cartilage thickness in the (a) talocrural surface of the talus, (b) posterior subtalar surface of the talus, and (c) posterior subtalar surface of the calcaneus. Error bars demonstrate 1 standard deviation.

region, respectively (Figs. 7 and 8) (Tables I and II). The thinnest articular cartilage (0–0.5 mm) in proximity mapping was found mainly in the anteromedial (14 of 16 tali) and anterolateral areas (13 of 16 tali).

In the posterior talar-subtalar surface, both mean and maximum cartilage thickness tended to be the largest in the central region (Figs. 7 and 8) (Tables III and IV). The thinnest articular cartilage (0–0.5 mm) was found mainly in the posterocentral (9 of 16 tali) and centro-medial areas (6 of 16 tali).

In the posterior calcaneal-subtalar surface, the cartilage thickness was more uniform than the other two (Figs. 7 and 8) (Tables V and VI). The thinnest articular cartilage (0–0.5 mm) was found mainly in the posterocentral (11 of 16 calcanei), and anterocentral and posterolateral areas (9 of 16 calcanei).

The average cartilage thickness of the anatomic section of the talocrural, talar-subtalar, and calcaneal-subtalar articular joint were 1.02 mm (range, 0.50–1.58 mm), 1.34 mm (range, 0.58–1.92 mm), and 1.04 mm (range, 0.58–1.48 mm), respectively. The optimum threshold for talocrural, talar-subtalar, and calcaneal-subtalar joint were 439 HU, 532 HU, and 480 HU, respectively (Table VII). When 439 HU for the talocrural, 532 HU for the talar-subtalar, and 480 HU for the calcaneal-subtalar joints were set as the optimum threshold, the mean measurement errors were 0.059 ± 0.066 mm, 0.038 ± 0.040 mm, and 0.018 ± 0.065 mm, respectively.

The canonical correlation coefficient was 0.995 ($P < 0.001$), which indicated that the subchondral bone plate threshold significantly correlated with the overlying anatomic cartilage thickness in the talocrural and subtalar joint.

Discussion

The present study experimentally determined the 3D distribution of articular cartilage thickness in the talocrural joint of the talus, the posterior subtalar joint of the talus, and that of the calcaneus in the elderly cadavers, and also showed the relationship between subchondral bone plate density and articular cartilage thickness for the elderly talus using 3D-CT and a 3D-digitizer[16].

Several studies have reported articular cartilage thickness and its distribution in the proximal talus[2,28–31]. Using an ultrasound system, Adam *et al.*[2] reported that the mean and maximum talocrural cartilage thickness in the elderly cadaveric talus (mean age; 82.5 ± 11.7 years) was 0.95 ± 0.17 mm and 1.68 ± 0.27 mm, respectively. They also described that the distribution pattern of talocrural cartilage thickness showed the thickest cartilage between the middle and posterior third of the weight-bearing surface. Using the *in vitro* needle probe technique, Shepherd *et al.*[28] reported that mean cartilage thickness (mean age; 65.1 ± 14.3 years) was 1.16 ± 0.30 mm. Millington *et al.*[29] analyzed the 3D-topography and thickness distribution of *in vitro* ankle articular cartilage (mean age; 61.5 years) by dissolving the articular cartilage with a stereophotographic technique, a type of 3D-digitizing system, and reported that the mean and maximum cartilage thickness was 1.10 ± 0.18 mm and 2.38 ± 0.4 mm, respectively. They also described that the thickest cartilage region occurred anterior-laterally and posterior-medially over the shoulders of the talus. In an *in vivo* study using a water-excitation magnetic resonance imaging (MRI) technique, Al-Ali *et al.*[30] reported a mean thickness of 0.89 ± 0.19 mm for the proximal talar cartilage layer in

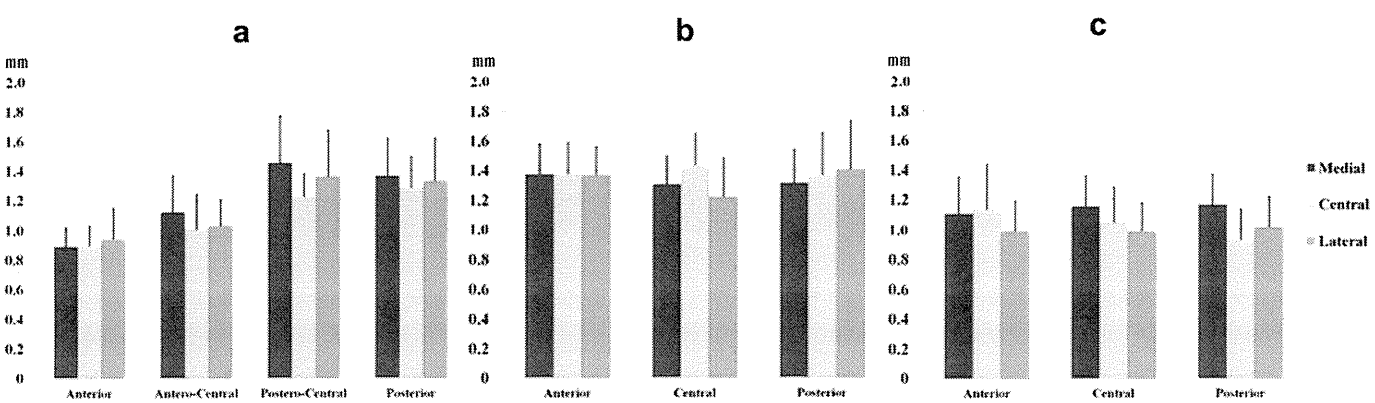

Fig. 8. Bar charts showing maximum cartilage thickness in the (a) talocrural surface of the talus, (b) posterior subtalar surface of the talus, and (c) posterior subtalar surface of the calcaneus. Error bars demonstrate 1 standard deviation.

Table I
Statistical comparison of mean cartilage thickness among each region in the talocrural joint of the talus

	AC-M	PC-M	PM	AC	AC-C	PC-C	PC	AL	AC-L	PC-L	PL
AM		***	***		*	***	***			***	***
AC-M		***	+			***	**			+	**
PC-M				**	*			***	***		
PM				***				***	***		
AC						***	***	*		***	***
AC-C						***	+	*			*
PC-C								***	***		
PC								***	***		
AL										***	***
AC-L										***	***
PC-L											**

AM, anteromedial; AC-M, anterocentral-medial; PC-M, posterocentral-medial; PM, posteromedial; AC, anterocentral; AC-C, anterocentral-central; PC-C, posterocentral-central; PC, posterocentral; AL, anterolateral; AC-L, anterocentral-lateral; PC-L, posterocentral-lateral; and PL, posterolateral.
GEE followed by a *post hoc* Bonferroni multiple comparison test.
Blank: $P \geq 0.1$; +: $P < 0.1$; *: $P < 0.05$; **: $P < 0.01$; ***: $P < 0.001$.

young volunteers (age 22–27 years). In another *in vivo* study using 1.5-T MRI with a fat-suppressed 3D spoiled gradient-recalled (SPGR) sequence, Wan *et al.*[31] described that the mean thickness of the proximal talar cartilage layers was 1.42 ± 0.18 mm in healthy young volunteers (age 24–42 years). They also reported that the thickest cartilage was in the posterolateral region and that there were significant differences between the posterior region and anterior or middle region in the lateral portion. Thus, because the talocrural cartilage is thin, measurement of talocrural cartilage thickness of the talus can depend on the measurement methodology as well as variance among subjects. Therefore, studies investigating thin cartilage (such as in the ankle) may need to conduct an accuracy test. In the present study, the mean cartilage thickness of the talocrural joint of the talus was 0.82 ± 0.12 mm and the mean measurement error was 0.059 ± 0.066 mm in the talocrural joint of the talus, thus denoting high accuracy. Therefore, the present evaluation of the distribution of talocrural articular cartilage thickness was validated.

Concerning the distribution pattern of cartilage thickness in the talocrural joint of the talus, the present findings showed that anterior regions were the thinnest with increasing cartilage thickness toward the posterior, in good agreement with Adam *et al.*[2]. The thickest cartilage regions in the talocrural surface of the talus were located in the posterocentral-medial and posterolateral region in the present study, in agreement with Millington *et al.*[29] and Wan *et al.*[31], respectively. Kurrat *et al.*[32] and Adam *et al.*[33] reported that fixation with formalin has no measurable effect on cartilage thickness or the geometric configuration of the joint using microscopic examination and ultrasonography, respectively. Therefore, the 3D distribution of the articular cartilage thickness in this study is further supported.

Table II
Statistical comparison of maximum cartilage thickness among each region in the talocrural joint of the talus

	AC-M	PC-M	PM	AC	AC-C	PC-C	PC	AL	AC-L	PC-L	PL
AM	**	***	***			***	***		+	***	***
AC-M		***	+	*							
PC-M				***	**			***	**		
PM				***	**			***	***		
AC						***	***		+	***	***
AC-C						**	*				
PC-C								***	***		
PC								***	***		
AL										**	*
AC-L										**	**
PC-L											

GEE followed by a *post hoc* Bonferroni multiple comparison test.
Blank: $P \geq 0.1$; +: $P < 0.1$; *: $P < 0.05$; **: $P < 0.01$; ***: $P < 0.001$.

Table III
Statistical comparison of mean cartilage thickness among each region in the posterior subtalar joint of the talus

	CM	PM	AC	C	PC	AL	CL	PL
AM				***	*			
CM				***				
PM				***				
AC					***		***	
C					***		***	**
PC						***		***
AL							***	
CL								**

CM, centro-medial; C, central; CL, centrolateral.
GEE followed by a *post hoc* Bonferroni multiple comparison test.
Blank: $P \geq 0.1$; +: $P < 0.1$; *: $P < 0.05$; **: $P < 0.01$; ***: $P < 0.001$.

To our knowledge, there has been no report on a distribution map of subtalar joint. A previous report described the cartilage thickness of subtalar joint using MRI[30], and reported that the mean cartilage thickness of the posterior subtalar joint of the talus and calcaneus was 0.72 ± 0.11 mm (0.55–0.97 mm) and 0.78 ± 0.12 mm (0.58–1.00 mm), respectively[30]. In the present study, the mean cartilage thickness was 0.98 ± 0.16 mm in the subtalar joint of the talus, and 0.75 ± 0.12 mm in that of the calcaneus; besides, the mean measurement errors of accuracy including 95% CI were 0.038 ± 0.040 mm and 0.018 ± 0.065 mm in the subtalar joint of the talus and calcaneus, respectively. Therefore, the present technique for measuring the subtalar joint was validated, and the cartilage thickness of the posterior subtalar joint of the talus was found to be significantly thicker than that of the calcaneus ($P < 0.001$). The distribution of cartilage thickness in the present study indicated that the thickest region tended to be the central in the talar-subtalar surface and the calcaneal-subtalar cartilage thickness was relatively uniform.

An interesting finding of this study is that in elderly specimens, the subchondral bone of the talocrural surface of the talus, the posterior subtalar surface of the talus, and that of the calcaneus had CT densities of approximately 439 HU, 532 HU, and 480 HU, respectively. According to a previous report[16], approximately 480 HU represented the density of subchondral bone plate in the femoral head with a mean age of 83 years (range, 64–97 years). This discrepancy in the CT density may be attributed to the difference between convex and concave joints. According to Duan *et al.*[34], the subchondral bone thickness in the concave side of facet joint (superior articular process) was thicker than that in the convex side (inferior articular process) for the lumbar facet joint of volunteers using MRI. Simkin *et al.*[35] found that subchondral bone

Table IV
Statistical comparison of maximum cartilage thickness among each region in the posterior subtalar joint of the talus

	CM	PM	AC	C	PC	AL	CL	PL
AM				**			*	
CM								
PM								
AC							*	
C							***	
PC							+	
AL							***	
CL								+

GEE followed by a *post hoc* Bonferroni multiple comparison test.
Blank: $P \geq 0.1$; +: $P < 0.1$; *: $P < 0.05$; **: $P < 0.01$; ***: $P < 0.001$.

Table V
Statistical comparison of mean cartilage thickness among each region in the posterior subtalar joint of the calcaneus

	CM	PM	AC	C	PC	AL	CL	PL
AM								
CM					**			
PM					***			*
AC								
C					**			**
PC								
AL								
CL								

GEE followed by a *post hoc* Bonferroni multiple comparison test.
Blank: $P \geq 0.1$; +: $P < 0.1$; *: $P < 0.05$; **: $P < 0.01$; ***: $P < 0.001$.

thickness at the concave side was thicker than that at the convex side in shoulder, elbow, wrist, hip, pretalar and first metatarsophalangeal joints using a fine contact radiograph of human cadavers. Therefore, compatible with the previous studies[34,35], it was found that the subchondral bone plate density was the largest in the posterior talar-subtalar joint. This could be because the talocrural surface of the talus and the posterior subtalar surface of the calcaneus are convex while that of the talus is concave.

It is also interesting that the anatomic cartilage thickness significantly correlated with the underlying subchondral bone plate density in the talus. Millington *et al.*[29] argued that the regions of greatest cartilage thickness correspond to regions in the ankle where the subchondral bone is most dense with reference to the findings of Muller-Gerbl and Putz[36] who investigated anatomical sections, in agreement with the findings of the present study. Adam *et al.*[2] discussed that the region of maximum cartilage thickness in the elderly ankle was located at the region where biomechanical investigations of the ankle using Fuji Prescale film have shown the highest contact stresses occur[37]. Though the role of subchondral bone change as a principal factor in OA progression is controversial, it can be said that the subchondral bone and cartilage influence each other strongly. Subchondral bone changes in OA are thought to be both a result and a cause of cartilage attrition. Therefore, the present findings on the relationship between subchondral bone plate density and cartilage thickness in the elderly specimens may lend deeper insight into the coupling of cartilage morphology and joint loading, which will assist clinicians in obtaining a better understanding of the ankle and subtalar joint and some of their disorders.

There are several potential limitations in this study. First, because the sample size was small, some obvious differences could fail to reach statistical significance. Second, no anthropometric data were obtained. Shepherd *et al.*[28] have reported a correlation ($r = 0.67$) between body mass index (BMI) and mean cartilage thickness of the ankle, which changed by 0.31 mm when the BMI changed by 10 kg/m^2. Thus, the absence of anthropometric data might not significantly influence on calculating the cartilage thickness in the elderly individuals. Third, although each specimen had its proper threshold (ranging from 298 to 708 HU), all specimens were not assessed with the proper threshold. Nevertheless, when 439 HU, 532 HU, and 480 HU were assumed as the optimum thresholds for the talocrural surface of the talus, the posterior subtalar surface of the talus, and that of the calcaneus, the mean measurement errors were 0.059 ± 0.066 mm, 0.038 ± 0.040 mm, and 0.018 ± 0.065 mm, respectively. Those findings validated the evaluation of articular cartilage thickness distribution using this method.

Table VI
Statistical comparison of maximum cartilage thickness among each region in the posterior subtalar joint of the calcaneus

	CM	PM	AC	C	PC	AL	CL	PL
AM								
CM					*	+		
PM				**	***	**	*	
AC						+		
C								
PC								
AL								
CL								

GEE followed by a *post hoc* Bonferroni multiple comparison test.
Blank: $P \geq 0.1$; +: $P < 0.1$; *: $P < 0.05$; **: $P < 0.01$; ***: $P < 0.001$.

Table VII
Proper and optimum threshold for subchondral bone plate in each articular joint

Specimen	Talocrural surface of the talus (HU)	Posterior subtalar surface of the talus (HU)	Posterior subtalar surface of the calcaneus (HU)
1	449	482	346
2	569	643	489
3	531	422	352
4	346	540	708
5	298	575	504
Average	439	532	480

There are several potential advantages in this study. First, osteochondral lesions (OCLs) of the talus such as osteochondral fracture or osteochondritis dissecans have been treated recently with autogenous transplantation of a cartilage-bone unit plug or reimplantation of cultured autogenous chondrocytes[38,39]. It can be helpful to know the standard thickness of the articular cartilage in the area where OCLs are common on the talar dome. Second, the complex anatomic and biomechanical properties of the ankle joint including the small weight-bearing surface and the high forces it needs to withstand, makes designing total ankle prostheses very challenging[40,41]. As the subchondral bone plate is an important factor governing orthopedic endoprostheses implantation[14,40], the present findings of the 3D cartilage thickness distribution representing the underlying subchondral bone density can help to understand the delicate structures of subchondral bone and to optimize the prosthetic implant design which warrants the resistance to weight-bearing in the ankle. Third, because the inferred cartilage thickness becomes thicker with increasing threshold values[16], it is important to evaluate articular cartilage thickness using CT arthrography at a constant optimum threshold. Understanding the optimum threshold of the subchondral bone of the ankle and subtalar joint can be used for *in vivo* precise measurement of 3D distribution of articular cartilage thickness of the ankle and subtalar joint using CT arthrography. Densities of 439 HU, 532 HU, and 480 HU on CT images were used for the subchondral bone contours of the talocrural, the posterior subtalar of the talus, and that of the calcaneus in the elderly individuals, respectively. Fourth, in computational biomechanical assessment of the foot and ankle using finite element models, incorporating an inhomogeneous cartilage thickness distribution rather than a homogenous distribution and more precise subchondral bone density in the elderly hindfoot may result in more precise computational analysis with real stress distribution around the articular cartilage[42].

Author contributions

All authors were involved in drafting the article critically for important intellectual content, and all authors approved the content of the manuscript. Takashi Sakai had full access to all of the data in the study and takes responsibility for the integrity of the data and the accuracy of the data analysis.

Study conception and design: Keisuke Akiyama, Takashi Sakai, Kazuomi Sugamoto.

Acquisition of data: Keisuke Akiyama, Takashi Sakai.

Analysis and interpretation of data: Keisuke Akiyama, Takashi Sakai, Norio Sugimoto, Hideki Yoshikawa, Kazuomi Sugamoto.

Conflict of interest

None.

Acknowledgments

The authors would like to thank Mr Akio Miyata, and Mr Kenji Harada for digitizing the specimens, Mr Yoshihiro Sakaguchi for obtaining the CT image, and Mr Ryoji Nakao for skillful technical support.

References

1. Sheehan FT, Seisler AR, Siegel KL. In vivo talocrural and subtalar kinematics: a non-invasive 3D dynamic MRI study. Foot Ankle Int 2007;28:323–35.
2. Adam C, Eckstein F, Milz S, Putz R. The distribution of cartilage thickness within the joints of the lower limb of elderly individuals. J Anat 1998;193:203–14.
3. Madry H, van Dijk CN, Mueller-Gerbl M. The basic science of the subchondral bone. Knee Surg Sports Traumatol Arthrosc 2010;18:419–33.
4. Eckstein F, Milz S, Anetzberger H, Putz R. Thickness of the subchondral mineralised tissue zone (SMZ) in normal male and female and pathological human patellae. J Anat 1998;192:81–90.
5. Milz S, Putz R. Quantitative morphology of the subchondral plate of the tibial plateau. J Anat 1994;185:103–10.
6. Milz S, Eckstein F, Putz R. Thickness distribution of the subchondral mineralization zone of the trochlear notch and its correlation with the cartilage thickness: an expression of functional adaptation to mechanical stress acting on the humeroulnar joint? Anat Rec 1997;248:189–97.
7. Botter SM, van Osch GJ, Waarsing JH, van der Linden JC, Verhaar JA, Pols HA, *et al.* Cartilage damage pattern in relation to subchondral plate thickness in a collagenase-induced model of osteoarthritis. Osteoarthritis Cartilage 2008;16:506–14.
8. Müller-Gerbl M. The subchondral bone plate. Adv Anat Embryol Cell Biol 1998;141:1–134.
9. Müller-Gerbl M, Putz R, Hodapp N, Schulte E, Wimmer B. Computed tomography-osteoabsorptiometry for assessing the density distribution of subchondral bone as a measure of long-term mechanical adaptation in individual joints. Skeletal Radiol 1989;18:507–12.
10. Radin EL, Rose RM. Role of subchondral bone in the initiation and progression of cartilage damage. Clin Orthop Relat Res 1986;213:34–40.
11. Chiba K, Ito M, Osaki M, Uetani M, Shindo H. In vivo structural analysis of subchondral trabecular bone in osteoarthritis of the hip using multi-detector row CT. Osteoarthritis Cartilage 2011;19:180–5.
12. Zhang ZM, Li ZC, Jiang LS, Jiang SD, Dai LY. Micro-CT and mechanical evaluation of subchondral trabecular bone structure between postmenopausal women with osteoarthritis and osteoporosis. Osteoporos Int 2010;21:1383–90.
13. Eckstein F, Müller-Gerbl M, Putz R. Distribution of subchondral bone density and cartilage thickness in the human patella. J Anat 1992;180:425–33.
14. Lubovsky O, Wright D, Hardisty M, Kiss A, Kreder HJ, Whyne C. Importance of the dome and posterior wall as evidenced by bone density mapping in the acetabulum. Clin Biomech (Bristol, Avon) 2011;26:262–6.
15. Buckland-Wright C. Subchondral bone changes in hand and knee osteoarthritis detected by radiography. Osteoarthritis Cartilage 2004;12:S10–9.
16. Akiyama K, Sakai T, Koyanagi J, Murase T, Yoshikawa H, Sugamoto K. Three-dimensional distribution of articular cartilage thickness in the elderly cadaveric acetabulum: a new method using three-dimensional digitizer and CT. Osteoarthritis Cartilage 2010;18:795–802.
17. Sokovic M, Kopac J. RE (reverse engineering) as necessary phase by rapid product development. J Mater Process Technol 2006;175:398–403.
18. Su B, Dhara S, Wang L. Green ceramic machining: a top-down approach for the rapid fabrication of complex-shaped ceramics. J Eur Ceram Soc 2008;28:2109–15.
19. Sahara W, Sugamoto K, Nakajima Y, Inui H, Yamazaki T, Yoshikawa H. Three-dimensional morphological analysis of humeral heads: a study in cadavers. Acta Orthop 2005;76:392–6.
20. Persson A, Andersson M, Oden A, Sandborgh-Englund G. A three-dimensional evaluation of a laser scanner and a touch-probe scanner. J Prosthet Dent 2006;95:194–200.
21. Neu CP, McGovern RD, Crisco JJ. Kinematic accuracy of three surface registration methods in a three-dimensional wrist bone study. J Biomech Eng 2000;122:528–33.
22. Materialize. Clinical. Available at: http://www.materialise.com. [accessed 19.07.2005].
23. Moritomo H, Murase T, Goto A, Oka K, Sugamoto K, Yoshikawa H. In vivo three-dimensional kinematics of the midcarpal joint of the wrist. J Bone Joint Surg Am 2006;88:611–21.
24. Besl PJ, Mackay N. A method for registration of 3-D shapes. IEEE Trans Patt Anal 1992;14:239–56.
25. Moritomo H, Viegas SF, Elder KW, Nakamura K, DaSilva MF, Boyd NL, *et al.* Scaphoid nonunions: a 3-dimensional analysis of patterns of deformity. J Hand Surg [Am] 2000;25:520–8.
26. Tabachnick BG, Fidell LS. Using Multivariate Statistics. 5th edn. Needham Heights, MA: Allyn & Bacon, Inc.; 2006.
27. Hardon DR, Szedmak S, Shawe-Taylor J. Canonical correlation analysis: an overview with application to learning methods. Neural Comput 2004;16:2639–64.
28. Shepherd DET, Seedhom BB. Thickness of human articular cartilage in joints of the lower limb. Ann Rheum Dis 1999;58:27–34.
29. Millington SA, Grabner M, Wozelka R, Anderson DD, Hurwitz SR, Crandall JR. Quantification of ankle articular cartilage topography and thickness using a high resolution stereophotography system. Osteoarthritis Cartilage 2007;15:205–11.
30. Al-Ali D, Graichen H, Faber S, Englmeier KH, Reiser M, Eckstein F. Quantitative cartilage imaging of the human hind foot: precision and inter-subject variability. J Orthop Res 2002;20:249–56.
31. Wan L, de Asla RJ, Rubash HE, Li G. In vivo cartilage contact deformation of human ankle joints under full body weight. J Orthop Res 2008;26:1081–9.
32. Kurrat HJ, Oberländer W. The thickness of the cartilage in the hip joint. J Anat 1978;126:145–55.
33. Adam C, Eckstein F, Milz S, Schulte E, Becker C, Putz R. The distribution of cartilage thickness in the knee-joint of old-aged individuals-measured by A-mode ultrasound. Clin Biomech 1998;13:1–10.
34. Duan CY, Espinoza Orías AA, Shott S, An HS, Andersson GB, Hu JZ, *et al.* In vivo measurement of the subchondral bone

thickness of lumbar facet joint using magnetic resonance imaging. Osteoarthritis Cartilage 2011;19:96–102.
35. Simkin PA, Graney DO, Fiechtner JJ. Roman arches, human joints, and disease: differences between convex and concave sides of joints. Arthritis Rheum 1980;23:1308–11.
36. Muller-Gerbl M, Putz R. 1st edn,In: Functional Anatomy of the Ankle Joint. The Tibial Pilon Fracture 1995;vol. 1. 3–25.
37. Bruns J, Rosenbach B. Pressure distribution at the ankle joint. Clin Biomech 1990;5:153–61.
38. Aurich M, Bedi HS, Smith PJ, Rolauffs B, Mückley T, Clayton J, *et al.* Arthroscopic treatment of osteochondral lesions of the ankle with matrix-associated chondrocyte implantation: early clinical and magnetic resonance imaging results. Am J Sports Med 2011;39:311–9.
39. O'Loughlin PF, Heyworth BE, Kennedy JG. Current concepts in the diagnosis and treatment of osteochondral lesions of the ankle. Am J Sports Med 2010;38:392–404.
40. Kakkar R, Siddique MS. Stresses in the ankle joint and total ankle replacement design. Foot Ankle Surg 2011;17:58–63.
41. van den Heuvel A, Van Bouwel S, Dereymaeker G. Total ankle replacement. Design evolution and results. Acta Orthop Belg 2010;76:150–61.
42. Cheung JT, Zhang M, Leung AK, Fan YB. Three-dimensional finite element analysis of the foot during standing–a material sensitivity study. J Biomech 2005;38:1045–54.

DETECTION OF ABNORMALITIES IN THE SUPERFICIAL ZONE OF CARTILAGE REPAIRED USING A TISSUE ENGINEERED CONSTRUCT DERIVED FROM SYNOVIAL STEM CELLS

Wataru Ando[1,2,3], Hiromichi Fujie[4,5], Yu Moriguchi[1], Ryosuke Nansai[4], Kazunori Shimomura[1], David A. Hart[2], Hideki Yoshikawa[1] and Norimasa Nakamura[1,6,7,*]

[1]Department of Orthopaedics, Osaka University Graduate School of Medicine, Suita, Osaka, Japan
[2]McCaig Institute for Bone and Joint Health, Faculty of Medicine, University of Calgary, Calgary, Alberta, Canada
[3]Department of Orthopaedics, Kansai Rosai Hospital, Amagasaki, Hyogo, Japan
[4]Biomechanics Laboratory, Department of Mechanical Engineering, Kogakuin University, Hachioji, Tokyo, Japan
[5]Biomechanics Laboratory, Faculty of System Design, Tokyo Metropolitan University, Hino, Tokyo, Japan
[6]Center for Advanced Medical Engineering and Informatics, Osaka University, Suita, Osaka, Japan
[7]Institute for Medical Science in Sports, Osaka Health Science University, Osaka, Japan

Abstract

The present study investigated the surface structure and mechanical properties of repair cartilage generated from a tissue engineered construct (TEC) derived from synovial mesenchymal stem cells at six months post-implantation compared to those of uninjured cartilage. TEC-mediated repair tissue was cartilaginous with Safranin O staining, and had comparable macro-scale compressive properties with uninjured cartilage. However, morphological assessments revealed that the superficial zone of TEC-mediated tissue was more fibrocartilage-like, in contrast to the middle or deep zones that were more hyaline cartilage-like with Safranin O staining. Histological scoring of the TEC-mediated tissue was significantly lower in the superficial zone than in the middle and deep zones. Scanning electron microscopy showed a thick tangential bundle of collagen fibres at the most superficial layer of uninjured cartilage, while no corresponding structure was detected at the surface of TEC-mediated tissue. Immunohistochemical analysis revealed that PRG4 was localised in the superficial area of uninjured cartilage, as well as the TEC-mediated tissue. Friction testing showed that the lubrication properties of the two tissues was similar, however, micro-indentation analysis revealed that the surface stiffness of the TEC-repair tissue was significantly lower than that of uninjured cartilage. Permeability testing indicated that the TEC-mediated tissue exhibited lower water retaining capacity than did uninjured cartilage, specifically at the superficial zone. Thus, TEC-mediated tissue exhibited compromised mechanical properties at the superficial zone, properties which need improvement in the future for maintenance of long term repair cartilage integrity.

Keywords: Cartilage tissue engineering; animal model; image analysis; mechanical properties; mechanical test; microstructure.

*Address for correspondence:
Norimasa Nakamura
Center for Advanced Medical Engineering and Informatics
Osaka University, 2-2 Yamadaoka, Suita
Osaka 565-0871, Japan
Telephone Number: +81-6-6879-3552
FAX Number: +81-6-6879-3559
E-mail: norimasa.nakamura@ohsu.ac.jp

Introduction

It is widely accepted that injuries to articular cartilage do not usually heal spontaneously due to their avascular surroundings and a variety of approaches have been tested to improve cartilage healing (Buckwalter, 2002; Hunziker, 2002). Among them, stem cell therapy could be a promising option to facilitate regenerative tissue repair. Mesenchymal stem cells (MSCs) have the capability to differentiate into a variety of connective tissue cells including bone, cartilage, tendon, muscle, and adipose tissue (Pittenger *et al.*, 1999). These cells may be isolated from various tissues such as bone marrow, skeletal muscle, synovial membrane, adipose tissue, and umbilical cord blood (De Bari *et al.*, 2001; Jankowski *et al.*, 2002; Lee *et al.*, 2003; Wickham *et al.*, 2003). MSCs isolated from synovial membrane may be well suited for cell-based therapies for cartilage because of the relative ease of their harvest and their strong capability for chondrogenic differentiation (De Bari *et al.*, 2001; Sakaguchi *et al.*, 2005; Ando *et al.*, 2007). Recent implantation studies have reported successful repair of cartilage defects using porcine synovial membrane-derived MSCs (Ando *et al.*, 2007; Koga *et al.*, 2008; Koga *et al.*, 2009).

As a potential MSC-based therapeutic method, we have developed a scaffold-free three-dimensional tissue-engineered construct (TEC) composed of allogenic MSCs derived from the synovium and extracellular matrices (ECMs) synthesised by the cells (Ando *et al.*, 2007; Ando *et al.*, 2008), and demonstrated the feasibility of the resultant TEC to facilitate cartilage repair in a large animal study (Ando *et al.*, 2007). Following implantation for 6 months, TEC efficiently repaired the chondral defects by developing a cartilage-like tissue without the development of any immunologic reaction, regardless of skeletal maturity (Shimomura *et al.*, 2010). However, more detailed observations revealed that more spindle shaped fibroblast-like cells were dominant in the superficial area of the repair tissue and this was not observed in normal cartilage (Ando *et al.*, 2007; Shimomura *et al.*, 2010). Therefore, it is important to evaluate the quality of repaired tissue in more detail, especially in the superficial zone area.

The function of articular cartilage is to support and distribute loads in joints and to minimise friction between opposing articular surfaces by the maintenance of lubrication. The adequate permeability of tissues is also

crucial for maintaining the cartilage by transportation of nutrients to chondrocytes in avascular cartilage (Maroudas *et al.*, 1968). In this regard, it is of significance to evaluate the micro-scaled mechanical properties, which are related to compression, lubrication, and permeability of normal and repair articular cartilage. The micro-scaled mechanical properties of *in vitro* engineered cartilaginous tissues have been investigated (Grad *et al.*, 2012). However, that study did not evaluate the properties of *in vivo* implanted tissue, and there have been no reports specifically on the micro-scaled biomechanical properties of the superficial zone of *in vivo* generated repair cartilage in a large-animal model.

In the present study, we have investigated the detailed structure and micro-mechanical properties of the cartilaginous tissue resulting from treatment with TEC in comparison with those of uninjured articular cartilage in a previously validated porcine model. The findings indicate that the superficial zone of the TEC-mediated repair cartilage is uniquely compromised compared to uninjured cartilage.

Material and Methods

Isolation and expansion of synovial mesenchymal stem cells (MSCs)

MSCs were isolated and expanded as previously reported (Ando *et al.*, 2007). Briefly, porcine synovial membranes were obtained aseptically from the knee joints of two four month old male domestic pigs (cross bred animals: Landrace/Yorkshire/Duroc) post-mortem within 12 h of death in accordance with a protocol approved by the institutional ethics committee. Synovial membrane specimens were taken from the area around the anterior cruciate ligament (ACL) of the knee, rinsed with phosphate buffered saline (PBS), minced meticulously, and digested with 0.4 % collagenase IV (Sigma-Aldrich, St. Louis, MO, USA) in high-glucose Dulbecco's modified Eagle's medium (DMEM; Gibco BRL/Life Technologies, Rockville, MD, USA) for 2 h at 37 °C. After neutralisation of the collagenase by growth medium containing DMEM supplemented with 10 % foetal bovine serum (FBS; HyClone, Logan, UT, USA) and 1 % Penicillin/Streptomycin (Gibco BRL/Life Technologies), the resulting cells were collected by centrifugation, washed with PBS, resuspended in the growth medium, and plated in culture dishes.

For expansion, the cells were cultured in the growth medium at 37 °C in a humidified atmosphere of 5 % CO_2, with the medium replaced once per week. After 15-28 days of primary culture, when the cells reached confluence, they were washed twice with PBS, harvested by treatment with trypsin-EDTA (0.25 % trypsin and 1 mM EDTA: Gibco BRL/Life Technologies) and then replated at 1:3 dilution for the first subculture. Cell passages were continued in the same manner with 1:3 dilution when they reached confluence. Cells at passages 4 to 7 were used in the present studies. Our previous studies indicated that cells cultured using the above-mentioned procedure were composed of mesenchymal stem cells by cell surface phenotyping (Ando *et al.*, 2007), therefore the cells were defined as MSCs in the present study.

Development of a basic TEC from MSCs

MSCs were plated on 6 cm diameter culture dishes at a density of 4.0 x 10^5/cm^2 in the growth medium with 0.2 mM ascorbic acid 2-phosphate (Asc-2P; Sigma-Aldrich). Within a day, the cells became confluent. After additional culture durations of 7 days, a monolayer complex of the cultured cells and an ECM synthesised by the cells developed, and this was detached from the substratum by application of shear stress at the cell-substratum interface using gentle pipetting. The detached monolayer complex was left in suspension to form a three-dimensional structure by active tissue contraction. This contracted tissue was termed a basic tissue engineered construct (TEC) (Fig. 1ab) (Ando *et al.*, 2007; Ando *et al.*, 2008).

Implantation of basic TEC into porcine chondral defects *in vivo*

The resultant TEC were prepared as an allograft without any chondrogenic stimulation. Four-month-old female domestic immature pigs (n = 6) were anaesthetised by intramuscular injection of a mixture of ketamine hydrochloride (50 mg/mL and 0.6 mL/kg of body weight) and xylazine (20 mg/mL and 0.3 mL/kg of body weight) and continuous intravenous injection of propofol (10 mg/mL and 8 mL/kg/h). After a medial parapatella incision, the medial femoral condyles of the both knees were exposed with the knee in deep flexion, and partial thickness chondral defects of 8.5 mm in diameter and 1.5-2.0 mm in depth, without penetrating the subchondral bone, were created using an electric router (Proxxon, Niersbach, Germany) and diamond disc grinding (Shofu, Kyoto, Japan). These chondral defects were considered to be comparable with ICRS grade III injury (http://www.cartilage.org/index.php?pid=223&lang=1) which is used in a clinical setting. In 4 of the 6 pigs, the basic TEC – which was left in suspension for up to 12 h until implantation – were implanted into the defect on one side of the knee without suturing (TEC-treated group). On the other side, the defects were left empty (Untreated group). In the other two pigs, the TEC was implanted in the defects on both sides and this group was add to the TEC-treated group (Ando *et al.*, 2007; Shimomura *et al.*, 2010). All animals were immobilised for 7 days with casting and then were allowed free cage activity. They were euthanised under anaesthesia at 6 months after surgery. Each graft site was divided into two parts. One was fixed and used for subsequent paraffin sectioning and histological analysis, and the other was subjected to mechanical testing including compression testing, friction testing, micro indentation testing, and permeability testing. Cylindrical specimens of 4 mm in diameter and 5 mm in depth were extracted for the mechanical tests. For comparison, cylindrically-shaped, uninjured cartilage-subchondral bone specimens of identical size were also extracted at a distance from the repair sites (uninjured group).

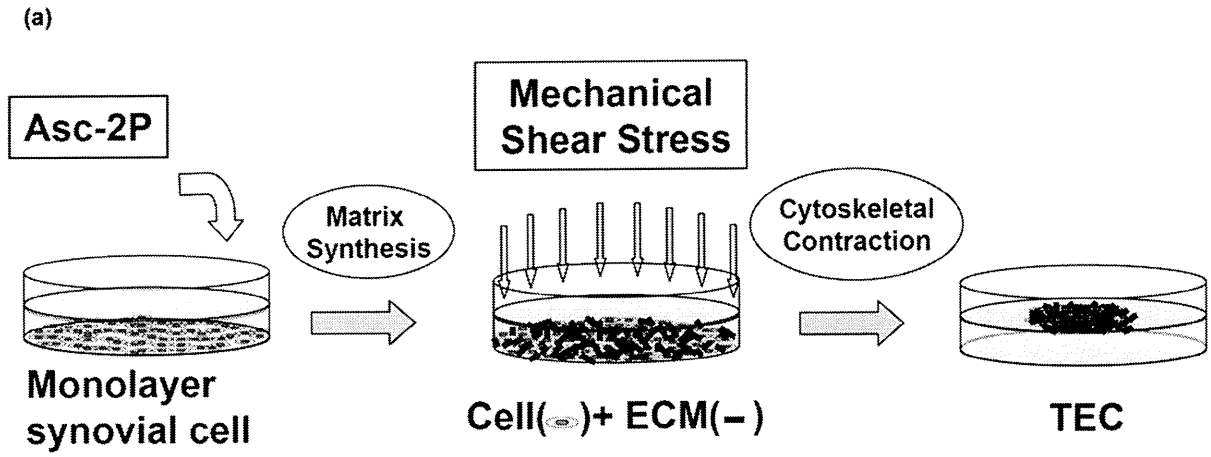

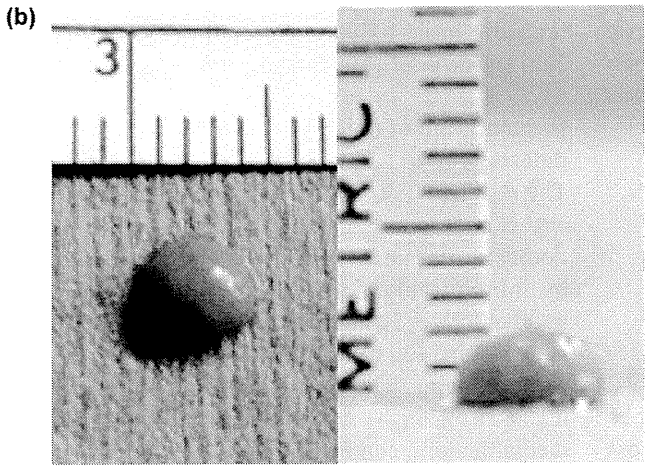

Fig. 1. Scheme of the development of TEC. **(a)** Schematic drawing of the development of TEC. To enhance extra cellular matrix (ECM) synthesis, ascorbic acid-2-phosphate was added to monolayer cultures of synovial MSCs. After culture durations of 7 days, a monolayer complex of the cultured cells and an ECM synthesised by the cells developed, and this was detached from the substratum by application of shear stress at the cell-substratum interface using gentle pipetting. The detached monolayer complex was left in suspension to form a three-dimensional structure by active tissue contraction. This contracted tissue was termed a basic tissue engineered construct (TEC). **(b)** Macroscopic view of the TEC, which was integrated to one spherical body. The diameter of this TEC was 5 mm and the thickness was 2 mm.

Histological and immunohistological analysis

Specimens were fixed with 4 % paraformaldehyde, decalcified with ethylene diamine tetraacetic acid (EDTA), and embedded in paraffin; 4 μm sections were stained with haematoxylin and eosin, as well as Safranin O. The repair tissue was divided into 4 parts of 2 mm width and each area was evaluated using the O'Driscoll scoring system (O'Driscoll, *et al.*, 1988). Each area was also divided into three parts corresponding to the superficial, middle and deep layers and evaluated by several criteria of the O'Driscoll scoring system including cellular morphology, Safranin O staining of the matrix, hypocellularity, and chondrocyte clustering. All scores for each area were averaged.

Picrosirius red was applied to serial sections and observed under polarised light microscopy to assess the collagen fibrils in the superficial layer of the repair tissue.

Serial sections were also subjected to immunohistochemical analysis. A polyclonal antibody (LPN) against proteoglycan 4 (PRG4; lubricin) (Schmidt *et al.*, 2009) was obtained through the courtesy of Dr John Sandy (Rush University, Chicago, IL, USA), and was used as the primary antibody. After the sections were incubated in 0.3 % H_2O_2 in 90 % methanol for 30 min at room temperature to block endogenous peroxidase activity, they were then incubated in 10 % normal goat serum. Next, the antibody LPN was applied to each section, followed by incubation overnight at 4 °C. Detection was then performed using the streptavidin biotin-peroxidase complex technique (Histofine SAB-PO Kit; Nichirei, Tokyo, Japan) before the sections were developed in 3,3-diaminobenzidine tetrahydrochloride (Dojindo Laboratories, Kumamoto, Japan) and counterstained with haematoxylin. Controls included no primary antibody assessments.

Macro-scale quasi-static compression testing

Macro-scale quasi-static unconfined compression testing was performed for each cylindrical specimen using a custom made compression tester (Katakai *et al.*, 2009). The quasi-static compression was applied to the specimen soaked in the saline solution at a rate of 4 μm/s to determine the bulk stiffness of the specimen in the linear region.

Scanning electron microscopy

Some cylindrical specimens were longitudinally sliced in the sagittal plane to yield specimens of 0.3 μm in thickness, using a microtome. Scanning electron microscopic (SEM) analysis was performed for each section specimen using the method developed by Katakai (Katakai, 2008). After dehydration in 50 % ethanol for 5 min, each specimen

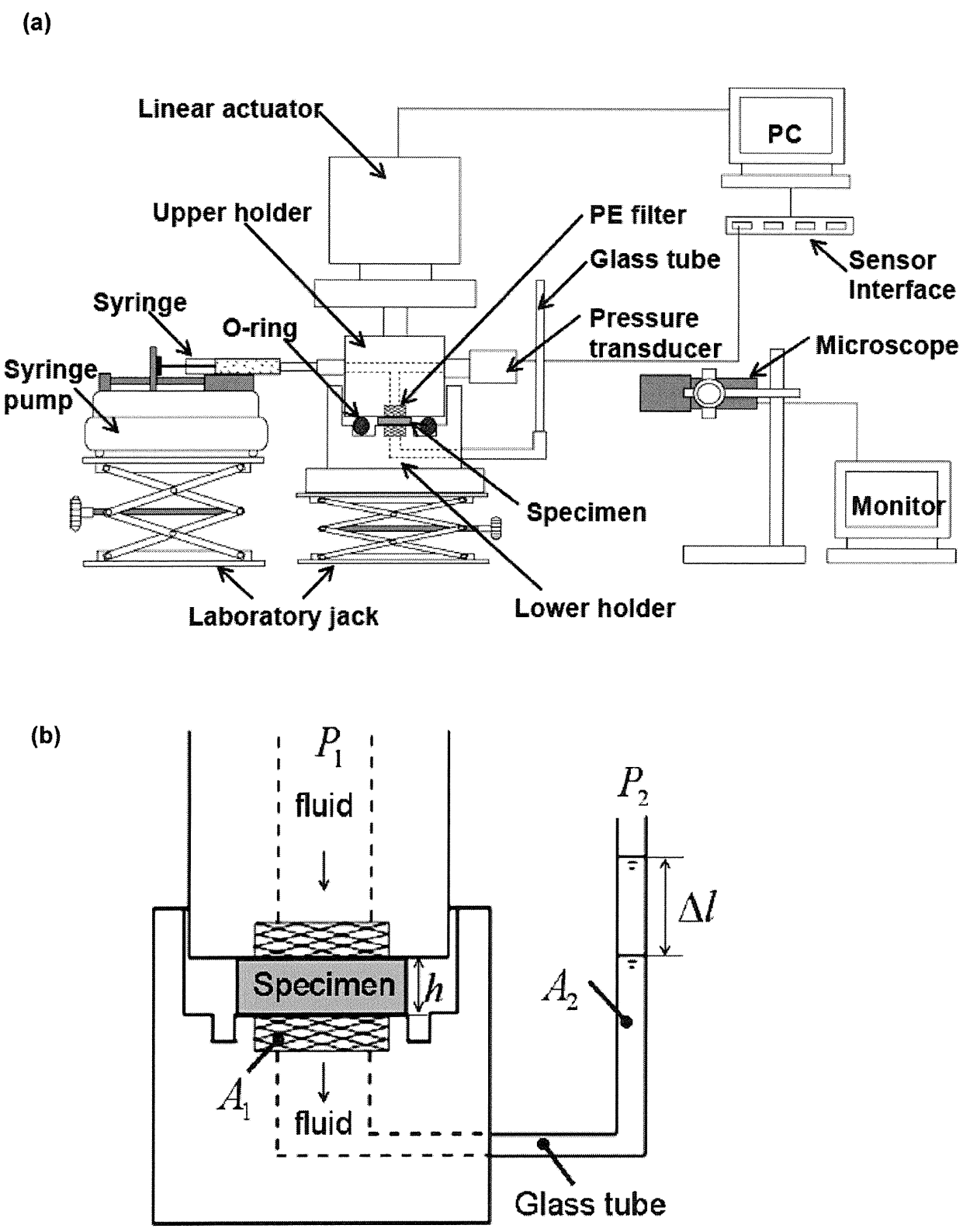

Fig. 2. Scheme of the device used for permeability testing. (a,b) Schematic drawing of the permeability testing apparatus used for assessment of cartilage layer-specimens. Sandwiched layer specimens of an initial thickness of h_0 was compressed with a strain of 30 % ($\varepsilon = 0.3$) in a saline solution at 37 °C. Under a hydrostatic pressure difference of 70 kPa (P_1-P_2), the outflow rate from the specimen $\Delta l/\Delta t$ was measured to determine the permeability of the specimen from the equation shown in the text, where A_1 represents the cross-sectional area of the specimen, while A_2 represents the cross-sectional area of the outflow capillary.

section was then further dehydrated in 70 % ethanol for 5 min and finally in 100 % ethanol for 5 min. Subsequently, it was fixed on a metal device and immersed in liquid nitrogen. SEM observation was performed for the specimens using a digital microscope (VE-8800, Keyence, Osaka, Japan) at an acceleration voltage of 1.5 kV and a magnification ratio of 15-700.

Atomic Force Microscopy observation and micro-indentation testing

An atomic force microscope (AFM) (Nanoscope IIIa, Veeco Instruments, Plainview, NY, USA) was used to examine structure-function relationships of uninjured cartilage and repaired tissues in the present study. AFM is a very high-resolution type of scanning probe microscopy, with demonstrated resolution on the order of fractions of a nm. It should be noted that not only geometry but also structural properties such as indentation stiffness can be obtained from uninjured cartilage and repair tissues without any specimen preparation (Kumar *et al.*, 2001; Fujie *et al.*, 2007; Nansai *et al.*, 2011).

Each cylindrical specimen (Uninjured cartilage; $n = 11$, TEC-treated tissue; $n = 7$, no-treated tissue; $n = 4$) was mounted on the sample stage of the AFM and soaked in saline solution at room temperature. Surface scanning was performed on the specimen using a contact mode of the AFM at a scan area of 30 x 30 μm and scan rate of 0.3 Hz using a silicon nitride probe (spring constant: 0.06 N/m, DNP-S, Veeco Instruments). From the obtained surface images, arithmetic surface roughness (R_a) was calculated using software installed in the AFM. Finally, a micro-indentation test was performed three times at 5 sites in each sample at an indentation rate of 5.12 μm/second and the values were averaged to determine the micro-scaled stiffness of the specimen. The distance between the sites assessed was always more than 1 mm. The stiffness of the superficial layer of uninjured cartilage and repair tissue, defined as the slope of the force-indentation curves between 300 and 400 nm of indentation, were subsequently obtained.

Friction testing

Reciprocal friction testing was performed for each cylindrical specimen using a friction tester developed in our laboratory (Ando *et al.*, 2007). The specimens were fixed to a probe edge of the tester so that the cartilage/cartilaginous repair tissue surface was uniformly attached to a glass plate soaked in saline solution at 37 °C. Sixty seconds after the application of vertical load of 1.76 N (140 kPa), the specimen was subjected to reciprocal friction at a rate of 20 mm/s with a stroke of 25 mm. Frictional force was measured with a custom-made cantilever-shaped load transducer with strain gauges having the rated output of 0.36 N and the non-linearity of 0.04 %. Coefficients of friction, defined as the ratio of frictional force to vertical load, were subsequently determined.

Permeability testing

For the permeability test, the cylindrical specimens used for the previous tests were transversely sliced to surface, middle, and deep layer specimens of approximately 300 μm in thickness, using a microtome. A permeability tester similar to that developed by Weiss *et al.* (Weiss *et al.*, 2006) was designed (Fig. 2ab). Each specimen of an initial thickness of h_0 was sandwiched between the top and bottom holders soaked in saline solution and then compressed with a strain of 30 % ($\varepsilon = 0.3$). A syringe pump was manually controlled for 1000 s so that the hydrostatic pressure difference P_1-P_2 was maintained at 70 kPa with a fluctuation of less than 2 kPa. The outflow rate from the specimen $\Delta l/\Delta t$ was measured and the permeability of the specimen, k was determined from the equation shown below based on Darcy's law (Mansour *et al.*, 1976), where A_1 represents the cross-sectional area of the specimen, while A_2 represents the cross-sectional area of the outflow capillary.

$$k = \frac{A_2 h_0 (1-\varepsilon)\Delta l}{A_1 (P_1 - P_2)\Delta t}$$

Note that no outflow was allowed from the lateral side of the specimen by means of an O-ring fixed into the tester around the specimen.

Statistical analysis

The results are presented as mean ± SD. In micro-indentation testing, friction testing, and permeability testing, the specimen numbers were 11 for uninjured cartilage, 7 for TEC-treated tissue and 4 for no-treatment repair tissue, and these results were analysed using analysis of variance (ANOVA) with Bonferroni's multiple comparison t-test in the STATVIEW version 5.5 software statistics package (SAS Institute, Cary, NC. USA). The results of the superficial thickness and histological scoring were analysed using unpaired t-tests and the Mann-Whitney U-test, respectively. Significance was set at $p < 0.05$.

Results

Overall histological and biomechanical evaluation of repair cartilage

When implanted with a TEC, the cartilage defects were repaired with a cartilaginous tissue with positive Safranin O staining in most of the repair tissue and such staining was also seen throughout the uninjured cartilage (Fig. 3ab). The untreated control defects were partially covered with a fibrous tissue with some evidence of osteoarthritic changes, associated with further loss of cartilage and erosion of subchondral bone (Fig. 3c). By O'Driscoll scoring, the TEC-mediated repair tissue had 62.5 % to 93.8 % values of the mean score of the uninjured cartilage in each category and the overall score was 18.1 ±3.7, which was 75.4 % of that of uninjured cartilage (score: 24) (Fig. 3d). For the histological scoring, all assessment criteria for the TEC-treated group were significantly higher than those for the untreated group, and also lower than that of uninjured group (Fig. 3d). The stress-strain relationships of the uninjured, TEC-treated and untreated specimens in the quasi-static compression test are shown in Fig. 3e. In the quasi-static compression test, the tangent modulus of the TEC-treated cartilage-like tissue was 1438.8 ±414.6 kPa,

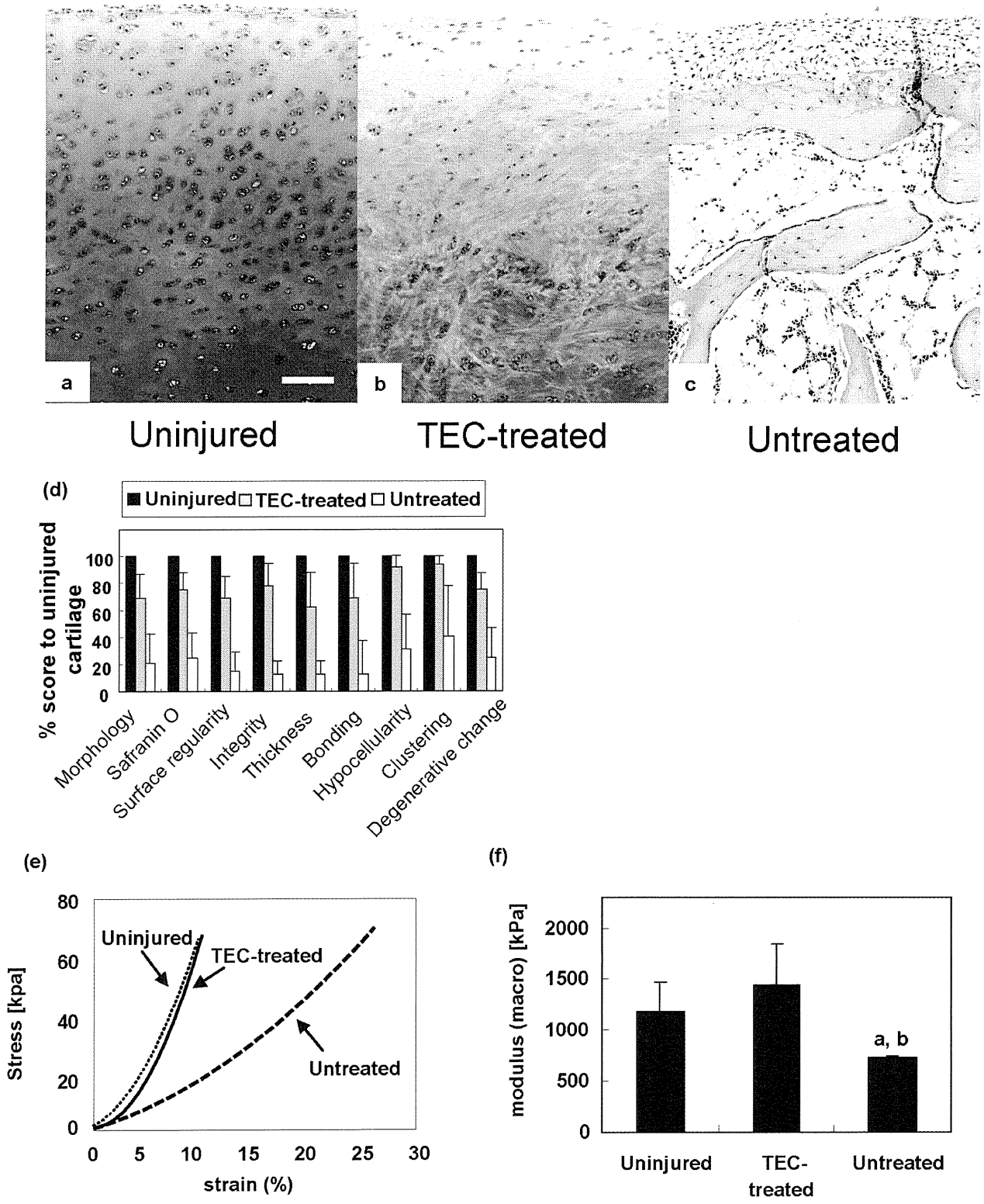

Fig. 3. Overall histological observations and biomechanical evaluation of TEC-mediated repair cartilage. **(a,b,c)** Safranin O staining of porcine uninjured normal articular cartilage **(a)** and chondral lesions treated with **(b)** or without **(c)** TEC at 6 months after implantation. Bar = 100 μm. **(d)** O'Driscoll histological and histochemical grading scale of uninjured articular cartilage (n = 12), repair tissue treated with (TEC; n = 8) and without treatment (Untreated; n = 4) TEC. **(e)** Typical stress-strain relationships of TEC-treated tissue compared with those of uninjured cartilage and untreated tissue. **(f)** Tangent modulus of uninjured cartilage (n = 10), the chondral lesion in the TEC treated group (n = 6) and those in the untreated group (n = 3) at compression rate of 4 μm/s. a: $p < 0.05$, compared to uninjured cartilage. b: $p < 0.05$ compared to the TEC treated group. There were no significant differences between the tangent modulus of TEC-mediated repair tissue and that of uninjured cartilage.

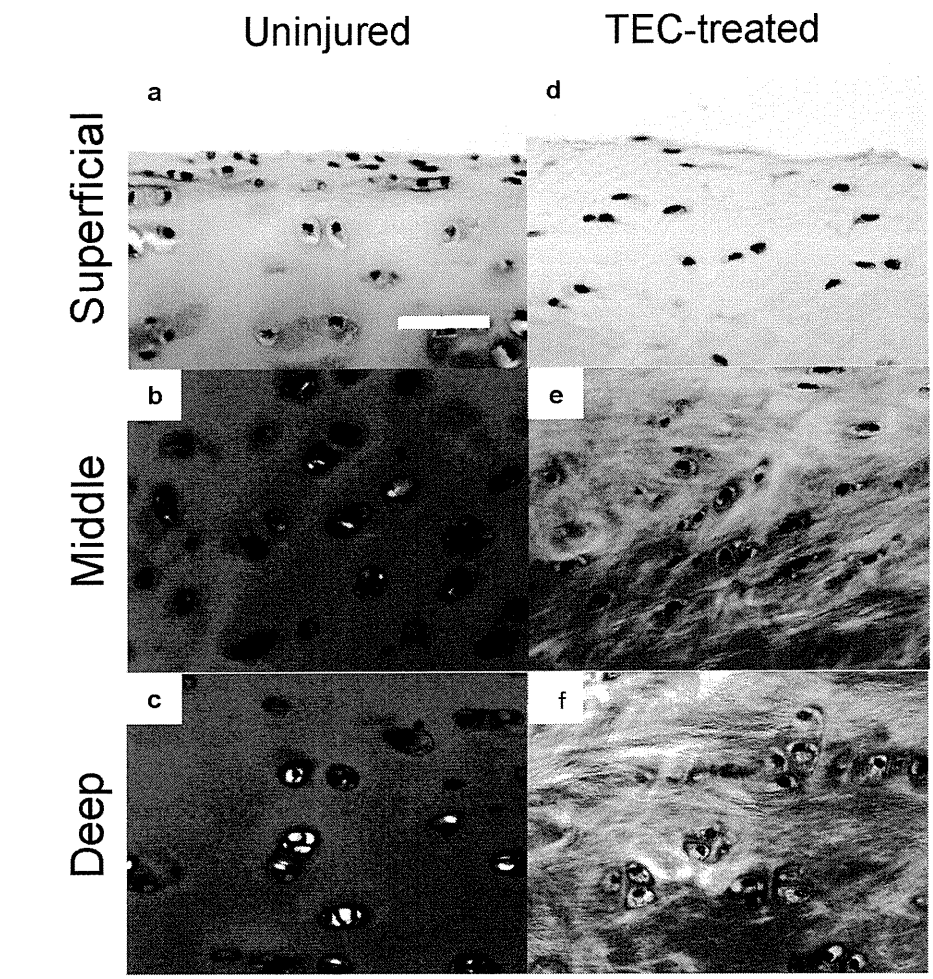

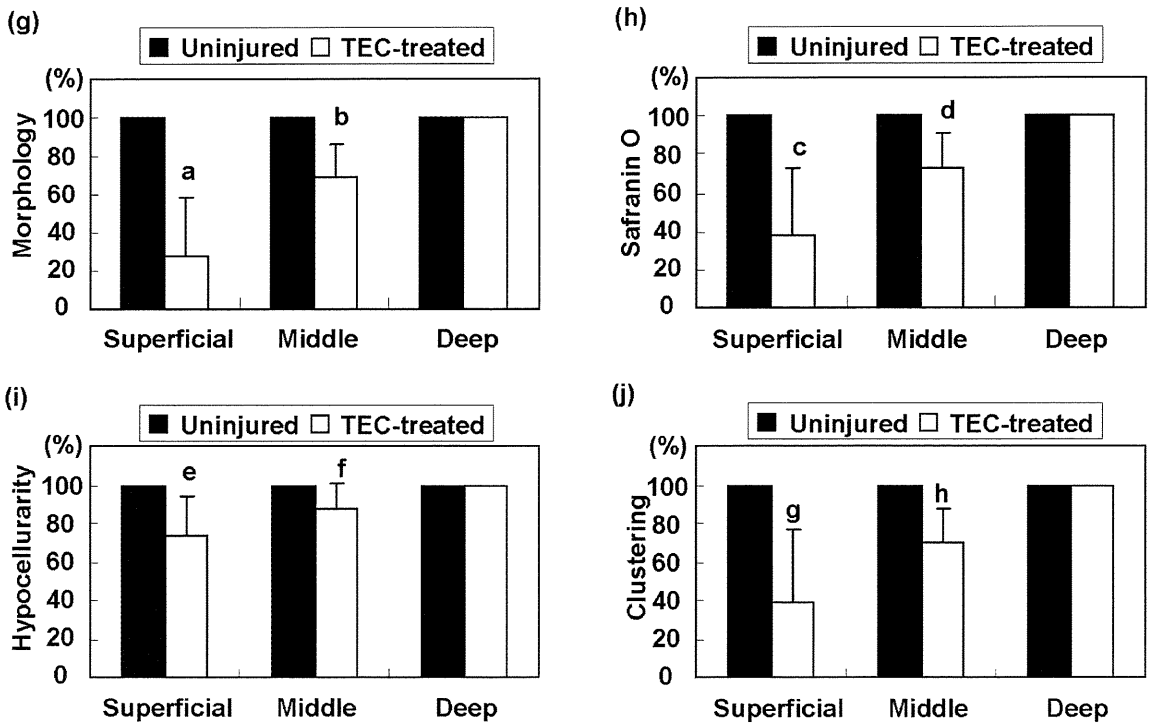

Fig. 4. Zonal histology of uninjured cartilage and the TEC-mediated repair cartilage. (a,b,c) Safranin O staining of superficial **(a)**, middle **(b)** and deep **(c)** zone of porcine chondral lesions 6 months after implantation of TECs. Bar = 25 μm. **(d,e,f)** Safranin O staining of superficial **(d)**, middle **(e)**, and deep **(f)** zone of uninjured cartilage. Bar = 25 μm. **(g,h,i,j)** Zonal histological and histochemical grading scale of uninjured articular cartilage and TEC-mediated repair tissue ($n = 8$). a,c,g: $p < 0.001$, b,d,h; $p < 0.01$, e,f; $p < 0.05$ compared to the uninjured cartilage.

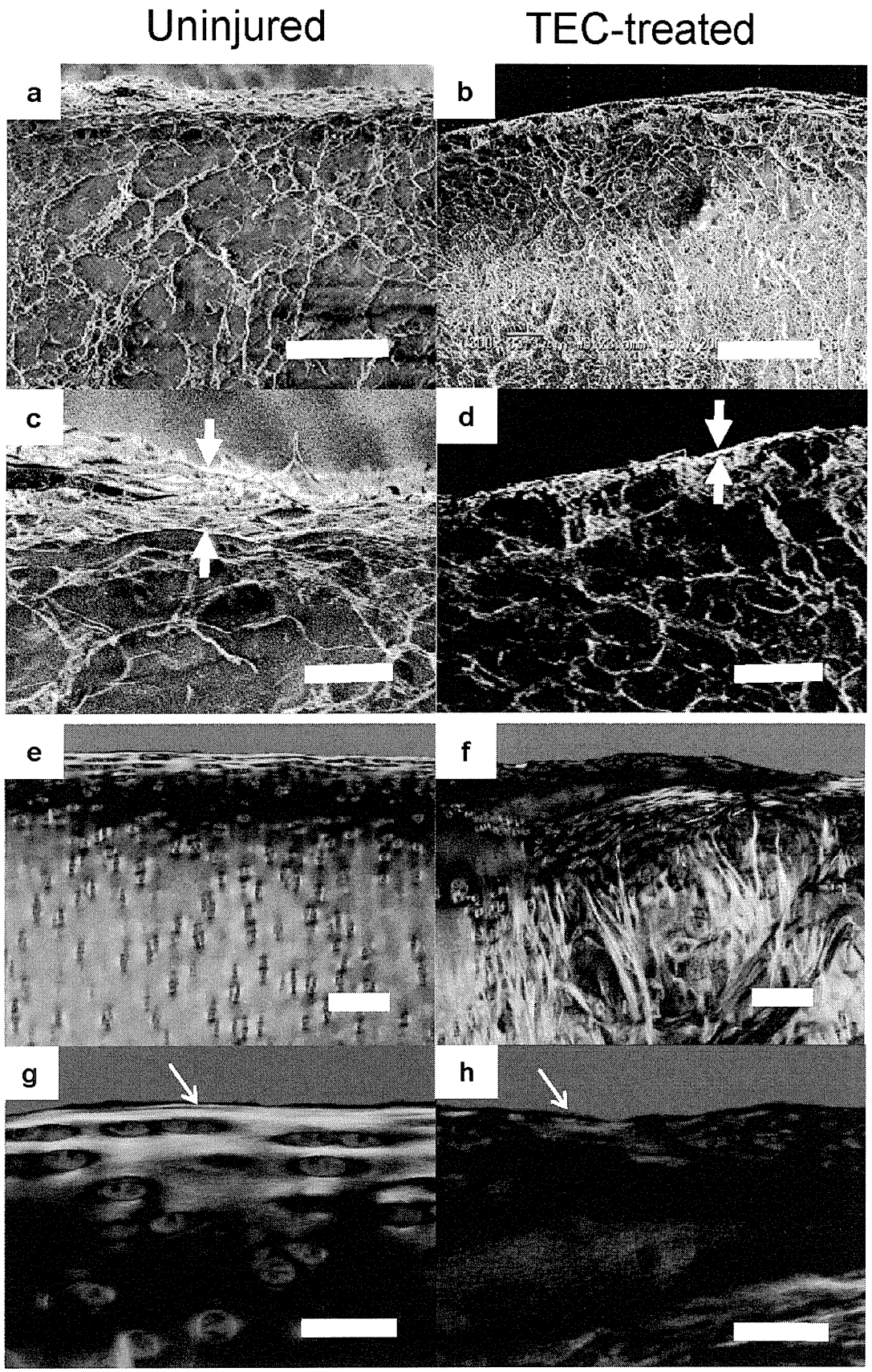

Fig. 5. Surface ultrastructure of repair cartilage. (a,b) Scanning electron microscopic (SEM) view of porcine normal **(a)** and chondral lesions treated with TEC at 6 months after implantation **(b)**. Bar = 100 μm. **(c,d)** Higher magnification SEM view of porcine uninjured cartilage (c) and chondral lesions treated with TEC (d). Bar = 25 μm. Arrow; the thickness of the superficial layer. **(e,f)** Polarised microscopic view of porcine uninjured (e) and chondral lesions treated with TEC (f). Bar = 200 μm. **(g,h)** Higher magnification polarised microscopic view of porcine uninjured (g) and chondral lesions treated with TEC (h). Bar = 50 μm. Arrows: one bright thin fibre was observed at the most superficial layer which has been termed the lamina splendens.

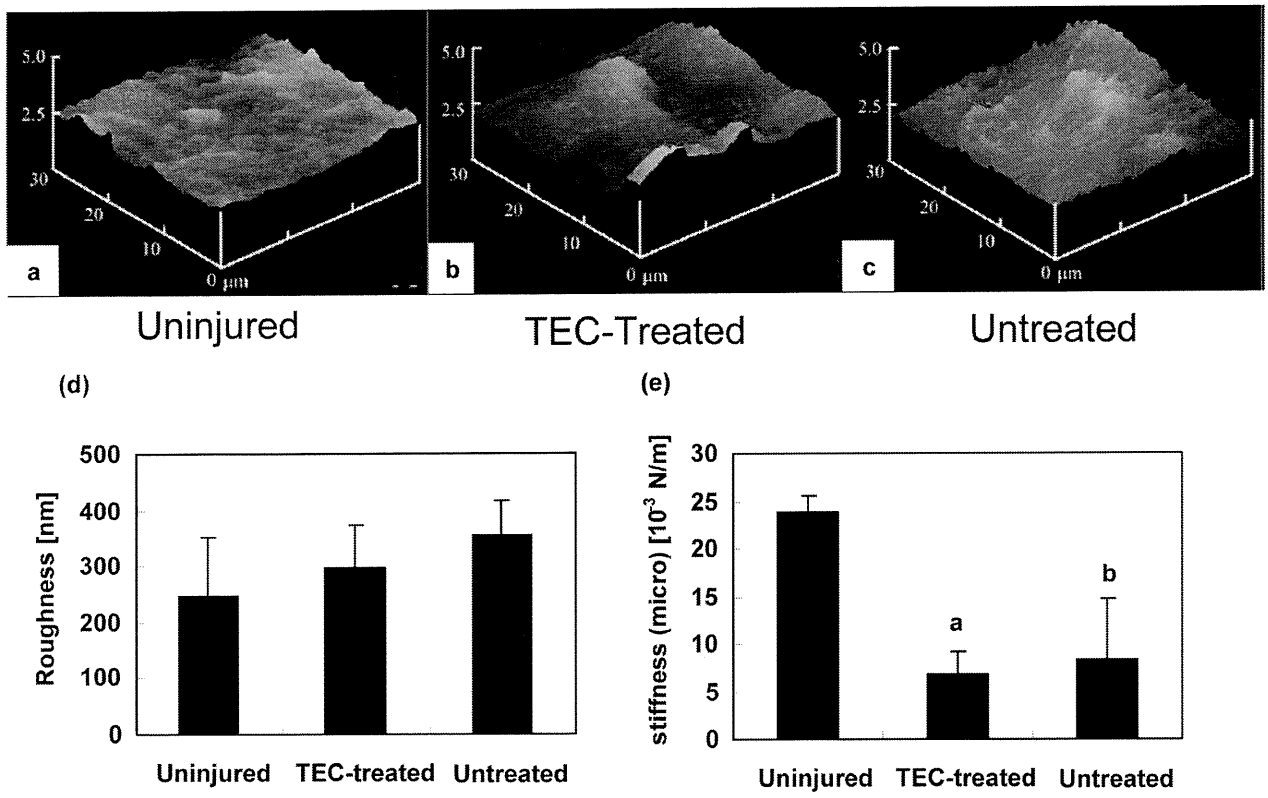

Fig. 6. Surface analysis of uninjured and TEC-mediated repair cartilage. (a,b,c) Atomic force microscopic (AFM)) view of porcine uninjured cartilage **(a)** and a chondral lesion treated with **(b)** or without **(c)** a TEC at 6 months after implantation. **(d)** The surface roughness of uninjured cartilage (n = 11), the chondral lesions in the TEC treated group (n = 7) and that in the untreated group (n = 4). **(e)** The surface stiffness of normal cartilage, the chondral lesions in the TEC treated group and that in the untreated group. a: $p < 0.05$, b: $p < 0.05$ compared to normal cartilage.

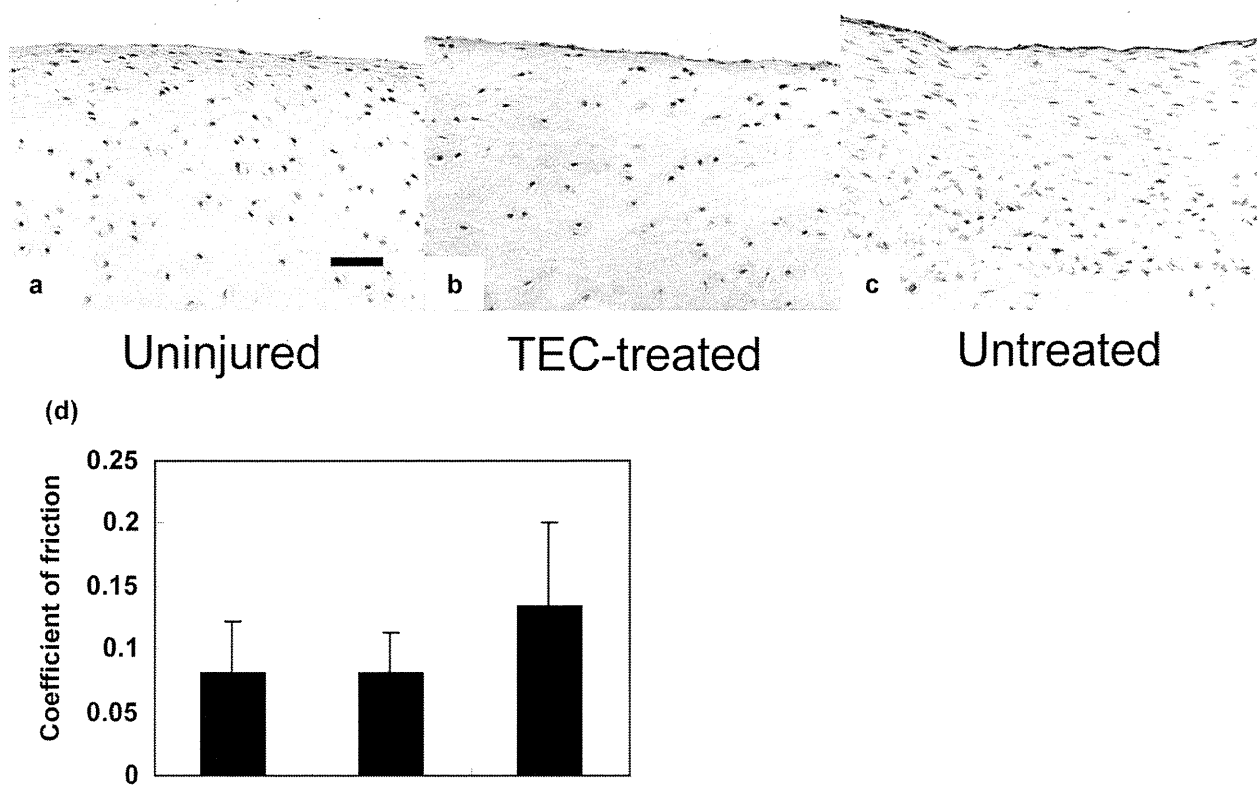

Fig. 7. Localisation of PRG4 in cartilage and lubrication properties. (a,b,c) Lubricin expression at the surface zone of uninjured **(a)** and chondral lesions treated with **(b)** or without **(c)** a TEC. **(d)** Frictional coefficient of uninjured cartilage (n = 11) and chondral lesions in the TEC treated group (n = 7) at 60 s with the application of a compressive force of 1.76 N. There were no significant differences between the frictional coefficients of repair tissue following implantation of a TEC and those of normal cartilage.

with no significant differences when compared to uninjured cartilage values (1182.0 ±297.0 kPa). In contrast, the tangent modulus of the untreated chondral defect tissue was 725.6 ±23.9 kPa, which was significantly lower than that of the TEC-treated cartilaginous tissue and uninjured cartilage (Fig. 3f).Thus, the TEC treated tissue had overall comparable values in morphology and biomechanical properties with those of uninjured cartilage.

Zonal histology of TEC-mediated repair cartilage

Zonal histological evaluation of the uninjured articular cartilage at higher magnification revealed that the most superficial area was a layer of fibrocartilage tissue lacking Safranin O staining (Fig. 4a). Most of the cartilage matrix beneath the fibrous layer was stained with Safranin O throughout the zones (Fig. 4abc). In the TEC-mediated repair cartilage, fibro-cartilaginous tissue was predominant in the superficial zone of the repair tissue lacking Safranin O staining (Fig. 4d) while most of the repair matrix in the middle and deep zones was composed of cartilaginous matrix with positive Safranin O staining (Fig. 4ef). By O'Driscoll histological scoring, the ratio of the score of the TEC-mediated repair tissue to that of uninjured cartilage was significantly lower in the superficial zone than in the middle and deep zone regarding the category of morphology, Safranin O staining, hypocellularity and chondrocyte clustering (Fig. 4ghij).

Surface ultrastructure of the TEC-mediated repair cartilage

SEM assessment revealed that there was a dense paralleled fibrous bundle at the most superficial layer of uninjured articular cartilage (Fig. 5a). Conversely, one thin layer covered the surface of the superficial zone of the TEC-mediated repair-cartilage (Fig. 5b). Higher magnification views revealed that the width of the dense paralleled fibrous bundle was approximately 20 μm. (Fig. 5c) while the one thin superficial layer of the TEC-mediated repair cartilage was approximately 2 μm (Fig. 5d). Picrosirius red staining revealed a bright orange band in the superficial layer of uninjured articular cartilage, of which the thickness was approximately 100-150 μm (Fig. 5e). It was notable that a red-coloured thin band with approximately 3 μm thickness was observed at the very surface of the orange band zone (Fig. 5g, arrow). Such a red band was not detected at the surface of the TEC-mediated repair tissue (Fig. 5f,h arrow).

Surface analysis of TEC-mediated repair cartilage

AFM analysis indicated that the surface of the uninjured cartilage consisted of bump-like protrusions of approximately 2 μm in height. The surface of the TEC-mediated and untreated cartilaginous tissues arising after injury exhibited a slightly rougher and a more irregular surface than that detected on uninjured cartilage (Fig. 6abc). The arithmetic surface roughness of the TEC-mediated cartilaginous tissue was 298 ±76.5 nm, which was a value between that of uninjured cartilage (247 ±103 nm) and the untreated cartilage-like tissue (354 ±61.7 nm), although no significant differences were detected between the three groups (Fig. 6d).

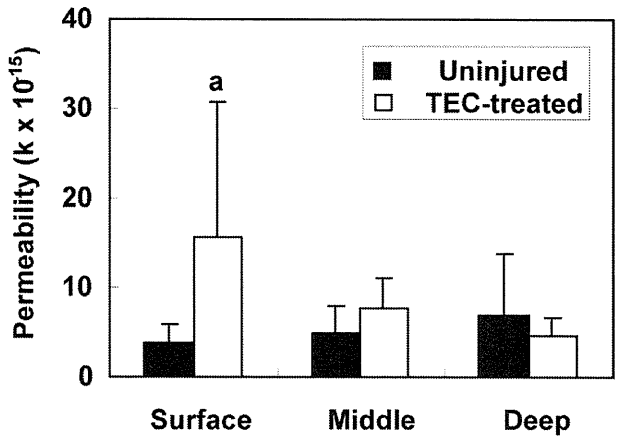

Fig. 8. TEC-mediated cartilage-like repair tissue exhibits low permeability at the superficial zone. Permeability of uninjured cartilage (n = 11) and chondral lesions in the TEC treated group (n = 7) at the surface, middle and deep zone. a: $p < 0.05$, compared to normal cartilage.

Micro-indentation testing showed that the surface stiffness of the TEC-mediated cartilaginous repair tissue was 6.79 ±2.30 x 10^{-3} N/m and the untreated cartilaginous tissues was 8.21 ±6.51 x 10^{-3} N/m, which were both significantly lower than values for uninjured cartilage (23.8 ±1.70 x 10^{-3} N/m) (Fig. 6e).

Localisation of PRG4 in TEC-mediated repair cartilage and lubrication properties

The proteoglycan 4 (PRG4) (lubricin) is considered to be the major protein responsible for the lubrication of articular cartilage (Swann *et al.*, 1977; Jay, 1992). PRG4 was localised to the surface of both uninjured and TEC-mediated repair cartilage, as well as the untreated repair tissue (Fig. 7abc). Friction testing indicated that the coefficient of friction for the TEC-mediated tissue was 0.081 ±0.033, with no significant differences observed between those of uninjured cartilage (0.081 ±0.041) and the untreated repair tissue (0.133 ±0.067) (Fig. 7b). The latter finding is likely due to the wide variability observed in the samples from the untreated group.

Permeability of the TEC-mediated repair cartilage

Permeability testing showed that the permeability of the TEC-mediated cartilage-like tissue was significantly higher than that of normal cartilage (18.6 ±15.7 x 10^{-15} m^4/Ns *vs.* 3.86 ±2.00 nm x 10^{-15} m^4/Ns) at the superficial zone, while there were no significant differences detected at the middle (6.63 ±3.26 x 10^{-15} m^4/Ns *vs.* 4.74 ±3.13 nm x 10^{-15} m^4/Ns) and the deep zones (4.67 ±2.00 x 10^{-15} m^4/Ns *vs.* 7.02 ±6.73 nm x 10^{-15} m^4/Ns) (Fig. 8). These results indicated that the middle to deep zones of the TEC-mediated repair cartilage had a fluid retention capacity similar to uninjured cartilage, while the superficial zone was more permeable than uninjured cartilage.